REPORT DOCUMENTATION PAGE

Form Approved
OMB No. 0704-0188

1. AGENCY USE ONLY (Leave blank)	2. REPORT DATE	3. REPORT TYPE AND DATES COVERED
	21 July 2002	Final Report, 1 July 1996 - 31 December 2001

4. TITLE AND SUBTITLE

Sensitivity and Adjoint Methods for Design of Aerospace Systems

5. FUNDING NUMBERS

(G) F49620-96-1-0329

6. AUTHOR(S)

John A. Burns

7. PERFORMING ORGANIZATION NAME(S) AND ADDRESS(ES)

Interdisciplinary Center for Applied Mathematics
Wright House, West Campus Drive
Virginia Polytechnic Institute and State University
Blacksburg, Virginia 24061-0531

8. PERFORMING ORGANIZATION REPORT NUMBER

ICAM Report 99-11-01

9. SPONSORING/MONITORING AGENCY NAME(S) AND ADDRESS(ES)

Air Force Office of Scientific Research
~~Code NM~~ Rm 713
~~801 North Randolph Street~~ 4015 Wilson Blvd
~~Arlington, VA 22203-1977~~ Arlington, VA 22203-1954

10. SPONSORING/MONITORING AGENCY REPORT NUMBER

AFRL-SR-AR-TR-03-
0322

11. SUPPLEMENTARY NOTES

12a. DISTRIBUTION/AVAILABILITY STATEMENT

Unlimited

Approved for public release,
distribution unlimited

12b. DISTRIBUTION CODE

13. ABSTRACT *(Maximum 200 words)*

This final technical report contains a summary and highlights of the research funded by the Air Force under AFOSR PRET Grant F49620-96-1-0329, titled "Sensitivity and Adjoint Methods for Design of Aerospace Systems". This research was conducted by the Air Force Center for Optimal Design and Control (**CODAC**), during the period 1 July 1996 to 31 December 2001. The Center conducts a wide range of research and educational programs, and promotes linkages between Air Force Laboratories, industry and university scientists. The PRET grant focuses on transition through industrial partnerships. During this period, **CODAC** researchers produced more than 115 scientific papers, made more than 150 presentations at conferences and colloquium and directed more than 20 graduate students and 7 postdocs. The research effort has produced several new computational tools for optimal design and these tools have already been transitioned into commercial software packages. Progress was made on a new sensitivity based method for estimating rotary stability derivatives. A new approach improved the efficiency of automatic differentiation when used in shape optimization. In the area of control, a new computational tool for controller reduction was devised and tested. This tool is based on proper orthogonal decomposition techniques. In addition, this report outlines some of the interactions between **CODAC**, industrial partners and Air Force facilities.

14. SUBJECT TERMS

Optimal Design of Fluids, Sensitivity Analysis, Flow Control, Scientific Computation

15. NUMBER OF PAGES
73

16. PRICE CODE

17. SECURITY CLASSIFICATION OF REPORT	18. SECURITY CLASSIFICATION OF THIS PAGE	19. SECURITY CLASSIFICATION OF ABSTRACT	20. LIMITATION OF ABSTRAC
Unclassified	Unclassified	Unclassified	UL

FINAL TECHNICAL REPORT ON AFOSR GRANT

F49620-96-1-0329

Sensitivity and Adjoint Methods for Design of Aerospace Systems

PRET

PARTNERSHIP FOR RESEARCH EXCELLENCE AND TRANSITION

THE AIR FORCE CENTER FOR OPTIMAL DESIGN AND CONTROL

for the period

1 July 1996 - 31 December 2001

by

John A. Burns, Director
Air Force Center for Optimal Design and Control

Wright House / West Campus Drive
Virginia Polytechnic Institute & State University
Blacksburg, VA 24061- 0531

July 31, 2002

Prepared for the : **Air Force Office of Scientific Research**
Mathematical & Computer Sciences
801 North Randolph Street
Arlington, VA 22203-1977

SENSITIVITY AND ADJOINT METHODS FOR
DESIGN OF AEROSPACE SYSTEMS

FINAL
TECHNICAL REPORT ON
AFOSR PRET Grant F49620-96-1-0329

Jeff Borggaard, John Burns, Eugene Cliff, Bernard Grossman, Belinda King
Interdisciplinary Center for Applied Mathematics
Virginia Polytechnic Institute and State University

John Lumley
Mechanical and Aerospace Engineering
Cornell University

Andrew Godfrey, William McGrory
AeroSoft, Inc.

Fritz Roetman
Boeing Defense and Space Group

1 Introduction and General Goals

This final technical report contains a summary of the activities supported under the Air Force AFOSR PRET Grant F49620-96-1-0329 during the period 1 July 1996 through 31 December 2001. This project was concerned with an interdisciplinary research program to develop and test new computational methods for optimization based design and sensitivity analysis of aerospace systems. The program integrated scientific and computational tools developed at **AeroSoft**, **Beam Technologies**, **Boeing Defense and Space Group** with new sensitivity techniques and optimization algorithms developed at **Virginia Tech** and **Cornell**. The focus of the program was fundamental research in sensitivity and adjoint based methods for design, control, and optimization of complex aerospace systems governed by partial differential equations. In addition, the program was structured to promote the transition of this basic research to Air Force laboratories and to industry. The principal investigator was Dr. John A. Burns. Hatcher Professor of Mathematics at Virginia Tech.

2 Introduction to the Center and General Research Goals

The *Air Force Center for Optimal Design and Control* (**CODAC**) was established in May 1993 under an Air Force AFOSR URI Grant. **CODAC** is an interdisciplinary research center with core academic participants at Virginia Tech. **CODAC** has made significant

progress in the areas of optimal design and control of systems governed by partial differential equations. In addition, **CODAC** has an established record of interactions with industry and Air Force laboratories. The current industrial partners include AeroSoft and Boeing Defense and Space Group. This group is composed of a proven team of scientists and engineers from small high-tech firms and major aerospace companies. In addition we have interactions with North carolina State University and Cornell University. These university groups furnishes valuable expertise in optimal design, control and optimization of a variety of application areas. The research group at Virginia Tech has been at the forefront of the development of sensitivity methods for optimal design, with applications to shape optimization for fluid flow management, and provides expertise in computational methods for optimization and for simulation of fluid dynamics. The industrial partners themselves contribute an immense expertise in computational fluid dynamics, finite element modeling and computational mechanics.

The effort supported under AFOSR PRET Grant F49620-96-1-0329 was built on a highly integrated interdisciplinary research program with three primary goals:

- To develop and investigate new mathematical and computational methods for sensitivity analysis with applications to optimal design of those aerospace systems described by nonlinear partial differential equations. These applications include (but are not limited to) shape optimization and design for flow management, materials processing, manufacturing, combustion and high speed flows. By working jointly with industrial partners and applying the results to real-world Air Force problems we established a direct and rapid track for transitioning new techniques and software to industry.

- The development of a mathematical foundation for the construction of new models and the investigation of the relationships between these models, simulation methods, sensitivity analysis and optimization algorithms. The objective is to provide a theoretical framework for the rigorous analysis of design algorithms that combine numerical simulation codes, approximate sensitivity calculations and optimization codes. In particular, it is important to determine under what conditions a given numerical simulation scheme can be combined with a specific optimization method to produce a convergent design algorithm.

- The development of a computational environment and high level software tools that engineers can effectively use to design and optimize aerospace systems. The objective is to initially provide a common software substrate to all university and industrial partners in the center and then develop this toolbox into a computational environment for design. The existence of this software tool will enable rapid dissemination of the technology developed in this project and help facilitate interactions between university researchers and industrial partners. The outcomes envisioned are new and practical computational tools for use in a wide range of aerospace design problems.

3 CODAC Organization and Facilities

Dr. John A. Burns is the *Director* of **CODAC** and is responsible for the day-to-day operations of the Center and for implementing and coordinating the research, laboratory/industry

interactions, and educational programs. *Dr. Eugene M. Cliff* is the *Director for Engineering.* **CODAC** is located within the Interdisciplinary Center for Applied Mathematics **(ICAM)** at Virginia Tech. *Dr. Terry Herdman* is the Director of **ICAM**. The *Executive Advisory Committee* consists of the Center Director, the Director for Engineering and the Director **ICAM**. The Executive Committee is responsible for program planning and for advising the Director on the allocation of resources and on ways to make **CODAC** more effective as an Air Force resource. The research conducted at **CODAC** requires computational, as well as more traditional laboratory facilities. Although much of the initial large scale computing was done on supercomputers at Air Force facilities, pre-processing and post-processing was done locally. During the past few years we have acquired an Origin 2000 supercomputer which enables us to develop practical software tools here at **ICAM**.

PRET Center Administration and Research Team

Research under the PRET Grant was conducted at six institutions: Virginia Tech, Cornell, AeroSoft, Beam Technologies, Boeing and Lockheed Martin. Frequent meetings of the team, exchange of visits, sharing of software, exchange of graduate students and postdocs, an annual industry-Air Force laboratory-university workshop and communication of results were be coordinated by the AFOSR-sponsored PRET Center **CODAC**. Professor John Burns, headed an advisory board which consisted of Walters (AeroSoft), Roetman (Boeing) and Grossman (MADD/Virginia Tech). Dr. Grossman was the Director of the Multidisciplinary Analysis and Design Center at Virginia Tech, has broad contact with the industrial aerospace design community.

The **PRET** Center provides the structure for unique educational and scientific training of students and post-doctoral researchers in an interdisciplinary team approach to scientific and engineering research. **CODAC** provided unique opportunities for theoretical, computational, and experimental research. Through the interactions with Air Force laboratories and industrial partners, students are exposed to real problems. The combined theoretical, computational, and experimental approach provides a meaningful interdisciplinary research experience.

ICAM Computing Facilities

ICAM houses a heterogeneous Unix system with file-sharing under a Network File System (NFS) and has excellent computational facilities. This includes:

- a 32-processor SGI Origin 2000 supercomputer with over 20 GB of RAM for large scale computing,
- a 4-processor SGI Origin 200 server providing NFS and NIS services,
- thirteen Unix workstations [SGI (9), DEC Alpha (2), Sun (2)],
- a collection of Pentium-based PC's (5) and Power-PC MacIntosh systems (4) with network access to the Unix systems and the Internet,

- a local (OC3) ATM network for NFS services and a (100 BaseT) switched Ethernet network for user services.

The research developed under this contract has wide applicability and promises considerable payoff in aerospace design applications. Although we worked with a variety of industrial groups, the interaction with AeroSoft Inc. was clear the most fruitful. This interaction will be detailed in the sections below.

lead to In order to provide focus for the research and to expedite its transition to industrial use we have developed research partnerships with the following groups:

Objectives

The research program had three primary objectives: (i) To develop and investigate new mathematical and computational methods for sensitivity analysis with applications to optimal design and control of aerospace systems; (ii) To develop a mathematical foundation for the construction of new models and to investigate the relationships between these models, simulation methods, sensitivity analysis and optimization algorithms; (iii) To develop a computational environment and high level software tools that engineers can effectively use to design and optimize aerospace systems. The goal was to provide a theoretical framework for the rigorous analysis of design algorithms that combine numerical simulation codes, approximate sensitivity calculations and optimization codes.

4 Accomplishments

Under the support of this grant we completed the development a suite of computational tools for sensitivity analysis, design, control, and optimization of a wide variety of nonlinear partial differential equations. We focused on the refinement of the hybrid continuous sensitivity methods that now form the foundations for the **AeroSoft** product *SENSE* and **Beam Technologies'** *CFETools*. We made considerable progress on algorithms for coupling single disciplinary sensitivity codes for application to multi-physics problems. This research has already been applied to COIL Laser design. In addition, we have completed an analysis of the role that sensitivities play in time marching numerical schemes and developed a new fast algorithm for solving optimal control problems governed by partial differential equations that arise in fluid flows. This work was motivated by interactions with our **Boeing** partners and the Air Vehicles Directorate of AFRL. Although this grant produced several major breakthroughs in sensitivity computations and optimal design, we will focus only on three major projects. These projects are summarized in the accomplishment section below. In addition, during this period the PRET Center has:

- Produced more than 115 scientific papers, articles and books,
- Made more than 150 presentations at conferences and colloquium,
- Directed more than 20 graduate students and 7 postdocs,

- Worked with more than 50 visitors, representing 10 different countries,
- Assisted in the development of AeroSoft's *SENSE* software package,
- Worked with several Air Force laboratories to transition the research into problems ranging from wind tunnel design to combustion control.

Major Accomplishments

We give a brief description of some research accomplishments and provide an indication of the significance and potential applications. details are given in the next section.

Accomplishment 1: Developed a Method for Estimating Stability Derivatives.

- **New Findings:** This extends work begun last year to the case of three-dimensional and viscous flows. The sensitivity equation provides an efficient way to compute static-stability derivatives which describe, in linear approximation, the way the aerodynamic forces and moments depend on the orientation of the body to the free-stream flow. This research is discussed in § ??.
- **Significance and Potential Applications:** While deducing some of these stability derivatives using finite-differences of neighboring solutions is possible, such methods may not be efficient. For example, in order to evaluate stability derivatives associated with asymmetric flight, nonlinear flow-solutions must be generated on an entire configuration, even in the usual case wherein the vehicle has a symmetry plane. The present approach allows one to compute derivatives, such as the weathercock stability parameter ($C_{n_\beta}|_{\beta=0}$), based on a nonlinear flow solution computed on one-half of the configuration.

Accomplishment 2: Discovered an Extreme Sensitivity in Nonlinear Boundary Value Problems of the Type that Describe Fluid Flows.

- **New Findings:** For convection diffusion problems we show that, because of finite precision arithmetic inherent in digital computers, convergent numerical algorithms can produce false (purely numerical) solutions. It is shown that these false solutions may be viewed as solutions of nearby problems with very high sensitivity to boundary values. In addition, because of this high sensitivity, mesh refinement to "converge a solution" only exacerbates the matter.
- **Significance and Potential Applications:** The above results show that "numerical based proofs" of non-uniqueness of solutions to hydrodynamic equations (e.g. Euler Equations) need further study. In particular, even convergent numerical schemes can produce false (non-unique) numerical solutions that are not solutions of the underlying

boundary value problem. This is extremely important when such codes are used for optimal design and control. This analysis also can be applied to the development of new accelerated marching algorithms. Finally, the sensitivity and stability analysis developed in this effort can be applied to more complex fluid flow phenomena. In particular, it supports the work of Bamieh, Butler, Dahleh, Farrell and Trefethen that suggest transition to turbulence in certain fluid flows are a result of flow sensitivity.

5 Technical Details

Here we present a few technical details concerning the accomplishments given above. These results may be found in the papers listed at the end of the report.

5.1 Direct Calculation of Aerodynamic Force Derivatives: A Sensitivity-Equation Approach

In this section we discuss the sensitivity-equation approach to computing stability derivatives using a single non-linear solution to the underlying fluid equations. The sensitivity equations are presented in integral form with the necessary boundary conditions. The lift-curve slope is computed at several angles of attack for a laminar airfoil. Stability characteristics are analyzed for the YB-49 flying wing.

5.1.1 Introduction

Computational Fluid Dynamics (CFD) plays an increasingly important role in the analysis and design of aerospace vehicles. From a flight mechanics view a primary purpose of CFD analyses is timely and accurate prediction of the aero-propulsion forces and moments applied to the vehicle. For control-system design we need to have some notion of how these forces and moments vary with vehicle motion - that is, one needs to estimate certain stability derivatives.

While deducing some of these stability derivatives using finite-differences of neighboring solutions is possible, such methods may not be efficient. For example, in order to evaluate stability derivatives associated with asymmetric flight, nonlinear flow-solutions must be generated on an entire configuration, even in the usual case wherein the vehicle has a symmetry plane. The present approach allows one to compute derivatives, such as the weathercock stability parameter $(C_{n_\beta}|_{\beta=0})$, based on a nonlinear flow solution computed on one-half of the configuration. In addition, certain derivatives (*e.g.* the damping-in-roll parameter C_{ℓ_p}), require a flow solution that permits explicit motions of the body (in this case roll-rate p). Such modeling may not be readily available in standard CFD codes.

In recent years the desire to use optimization-based design algorithms has spurred the need for design sensitivities and for efficient ways to calculate them. At this point there are three approaches to the calculation of design sensitivities:

1. finite difference of neighboring solutions

2. 'differentiate' the numerical code (*i.e.,* ADIFOR)

3. 'differentiate' the boundary-value problem

While there are subtleties, in the second approach formally one imagines applying the chain-rule to each line of code to produce another code which will evaluate the derivatives. Here we will focus on the third approach, often called the Sensitivity Equation Method (SEM). A high-level view of the abstract SEM approach is that it produces a *linear* boundary-value problem; the solution of this problem is a flow sensitivity and describes, in linear approximation, the way the flow solution (dependent variables) depends on a (scalar) design parameter. In applications one finds that the solution of the underlying nonlinear boundary-value problem often relies on a linearization so that many of the required ingredients for the SEM already exist within the basic CFD code.

A related approach applies the SEM to the *discretized* equations. This is also related to the ADIFOR approach, in that both are applied to a discretized problem. In general a discrete approximation of the linear SEM is not the same as applying sensitivity ideas to the discrete equations. For one thing, the latter approach requires grid sensitivities which need not arise in the abstract method. There are connections between these approaches, including a notion of *asymptotic consistency* develped under the present research.

In this section we will develop and demonstrate the abstract SEM method for computing stability derivatives. Thus, we must formulate the flow equations so that the desired flight parameters, such as angle-of-attack and side-slip angle, are available explicitly. Thus, the following discussion is devoted to the parameterization of the body geometry and to a careful description of some underlying coordinate systems. Following this we will briefly describe the flow-equations and the associated boundary conditions. The main contribution is the derivation of sensitivity equations for this class of problems. We demonstrate the approach with several examples.

5.1.2 Body Geometry

In CFD applications the problem geometry is commonly described in terms of a grid. Abstractly, one imagines a map from a computational domain to the physical domain and the grid provides a discrete version of this map. The body geometry is implicitly described by imposing appropriate boundary conditions on specific planes or parts of planes in the computational domain.

For our purposes we must describe how the body moves and/or deforms under specific changes in the geometry. Since we are concerned with relative motions between the body and the surrounding fluid, there are inevitably several reasonable choices for underlying coordinates. Our approach is arguably natural from a flight mechanics point-of-view.

We assume the atmosphere is homogeneous and at rest and use the symbol $\vec{\mathbf{V}}_c$ to denote the lineal velocity of a specified point on the vehicle. At this specified point we imagine two coordinate systems with a common origin

- a local horizontal system $Ox_h y_h z_h$, and
- a body-fixed system $Ox_b y_b z_b$.

The local horizontal system has the Ox_hy_h horizontal with z_h vertical and down. Since the atmosphere is homogeneous and at rest we can take $\vec{\mathbf{V}}_c = [1,\ 0,\ 0]_h^T$, so that the basic translational motion is in the x_h direction. Because of this choice, the body-fixed system $Ox_by_bz_b$ is oriented to the horizontal system by the aerodynamic angles: α, the angle-of-attack; and β, the sideslip angle.

The jig-shape of the vehicle is defined by a map $\pi_o : \Sigma \subset \mathbb{R}^2 \mapsto \mathbb{R}^3$. Here $\sigma \in \Sigma$ are points in the computational plane that define the body boundary or a part of the body. In applications, one does not deal with the map π_0 but rather with the image points produced - that is, the points of the physical domain that correspond to appropriate boundary points in the computational domain. In applying the abstract SEM, we will need to compute various partial derivatives so that we must describe explicitly the underlying maps.

We are concerned with changes in the flow field (and so, changes in the applied loads) that are induced by deformations and motions of the body. For body deformations we admit a deformation field π_1 so that points on the surface of the deformed body are given by

$$\vec{r}_s(\sigma, \phi_1) = \vec{\pi}_o(\sigma) \ + \ \phi_1 \vec{\pi}_1(\sigma), \tag{5.1}$$

where the scalar ϕ_1 is the magnitude of the deformation. It is possible to admit a combination of deformations $\pi_1, \pi_2, \ldots$, but since we deal with these one at a time the single deformation case is adequate. In design applications the field π_1 would describe a perturbation of interest, for example, geometric twist distribution in a wing. In aeroelastic applications, the field would describe some elastic mode - the SEM then gives a direct calculation of the associated aeroelastic stiffness parameter.

5.1.3 Integral Equations for Fluid Dynamics

The scope of this paper encompasses both inviscid and viscous flow fields. Solutions to the fluid-dynamic equations provide coefficients for the sensitivity equations which are discussed below. The three-dimensional flow of a calorically-perfect, viscous fluid is governed by a system of non-linear, hyperbolic partial differential equations which can be written in integral form as

$$\frac{\partial}{\partial t} \iiint \mathbf{Q}\, dV + \oint_A (\mathbf{F}(\mathbf{Q}) \cdot \hat{\mathbf{n}})\, dA = \oint_A (\mathbf{F}_v(\mathbf{Q}) \cdot \hat{\mathbf{n}})\, dA. \tag{5.2}$$

The conservative variables are $\mathbf{Q} = \mathbf{Q}(x, y, z, t) = [\rho, \rho u, \rho v, \rho w, \rho e_0]^T$ and represent the density, momentum and total energy per unit volume of the fluid. The surface integrals represent the inviscid and viscous fluxes ($\mathbf{F}$ and $\mathbf{F}_v$). Transport properties are computed using Sutherland curve fits. The integral formulation is the fundamental starting place for finite-volume discretizations.

This system of equations may be solved subject to boundary conditions which for an inviscid flow involve scalar relationships such as

$$\vec{\mathbf{V}} \cdot \hat{\mathbf{n}} \ = \ 0 \tag{5.3}$$

$$\nabla f \cdot \hat{\mathbf{n}} \ = \ 0, \tag{5.4}$$

where the velocity vector is depicted as $\vec{\mathbf{V}} = (u, v, w)^T$. For a viscous fluid, the no-slip condition is simply $\vec{\mathbf{V}} = 0$.

While the model Eqn. (5.2) includes explicit time-dependence, we are interested only in the steady-state solution, which is assumed to exist. For this purpose we introduce the notation

$$\tilde{\mathbf{Q}}(x,y,z) \equiv \lim_{t\to\infty} \mathbf{Q}(x,y,z,t).$$

5.1.4 Sensitivity Equations

The idea of a flow sensitivity is that of a linear approximation – loosely a partial derivative of the flow with respect to a parameter of interest. Here we use the symbol η to denote a generic parameter and to emphasize that the flow solution depends both on position in space and on the parameter we write

$$\tilde{\mathbf{Q}}(x,y,z;\eta).$$

The sensitivity we seek is then formally given by

$$\mathbf{S} \equiv \frac{\partial \tilde{\mathbf{Q}}}{\partial \eta}. \tag{5.5}$$

Our objective is to derive a linear boundary-value problem for $\mathbf{S}(\cdot;\eta)$. We do this formally, by differentiating the elements of the nonlinear boundary-value problem for the flow $\tilde{\mathbf{Q}}(\cdot;\eta)$. Here we are specifically interested in two parameters:

- α – the angle-of-attack, and
- β – the side-slip angle.

5.1.5 Finite-Volume Sensitivity

Our form of the governing equations in Eqn. (5.2) is valid in an inertial reference frame. In particular, we choose a frame such that the Cartesian-coordinate axes agree with with the instantaneous body axes (jig shape). The parameters of interest (α,β) then do not explicitly appear in any of the flux functions. In this case we proceed by formally differentiating Eqn. (5.2) with respect to η and then interchange orders of differentiation to find

$$\frac{\partial}{\partial t}\iiint \mathbf{S}\, dV + \oint_A \left(\mathbf{F}'(\tilde{\mathbf{Q}},\mathbf{S})\cdot\hat{\mathbf{n}}\right) dA = \oint_A \left(\mathbf{F}'_v(\tilde{\mathbf{Q}},\mathbf{S})\cdot\hat{\mathbf{n}}\right) dA, \tag{5.6}$$

where $\tilde{\mathbf{Q}}$ represents the conservative variables available from the steady-flow solution and $\mathbf{S}$ represents the unknown flow sensitivities. Note that the governing equations for $\mathbf{S}(\cdot;\eta)$ is linear and that the flow solution ($\tilde{\mathbf{Q}}(\cdot,\eta)$) enters through spatially varying coefficients. We have previously demonstrated that in the Euler flow case, Eqn. (5.6) is equivalent to computing the η-derivative of the differential form of the conservation law.

The inviscid flux vector in the sensitivity equations is written as

$$\mathbf{F}'\cdot\hat{\mathbf{n}} = \frac{\partial \mathbf{F}}{\partial \mathbf{Q}}\frac{\partial \mathbf{Q}}{\partial \eta}\cdot\hat{\mathbf{n}} \equiv \frac{\partial \mathbf{F}}{\partial \mathbf{Q}}\mathbf{S}\cdot\hat{\mathbf{n}} = \left\{\begin{array}{c} \rho'(\vec{\mathbf{V}}\cdot\hat{\mathbf{n}}) + \rho(\vec{\mathbf{V}}'\cdot\hat{\mathbf{n}}) \\ \rho' u(\vec{\mathbf{V}}\cdot\hat{\mathbf{n}}) + \rho u'(\vec{\mathbf{V}}\cdot\hat{\mathbf{n}}) + \rho u(\vec{\mathbf{V}}'\cdot\hat{\mathbf{n}}) + \hat{n}_x p' \\ \rho' v(\vec{\mathbf{V}}\cdot\hat{\mathbf{n}}) + \rho v'(\vec{\mathbf{V}}\cdot\hat{\mathbf{n}}) + \rho v(\vec{\mathbf{V}}'\cdot\hat{\mathbf{n}}) + \hat{n}_y p' \\ \rho' w(\vec{\mathbf{V}}\cdot\hat{\mathbf{n}}) + \rho w'(\vec{\mathbf{V}}\cdot\hat{\mathbf{n}}) + \rho w(\vec{\mathbf{V}}'\cdot\hat{\mathbf{n}}) + \hat{n}_z p' \\ \rho' h_0(\vec{\mathbf{V}}\cdot\hat{\mathbf{n}}) + \rho h_0'(\vec{\mathbf{V}}\cdot\hat{\mathbf{n}}) + \rho h_0(\vec{\mathbf{V}}'\cdot\hat{\mathbf{n}}) \end{array}\right\}, \tag{5.7}$$

where the density sensitivity is ρ', the velocity sensitivity is $\vec{\mathbf{V}}' = (u', v', w')^T$, and the pressure sensitivity is p'. The stagnation enthalpy per unit mass is defined as $h_0 \equiv h + (\vec{\mathbf{V}} \cdot \vec{\mathbf{V}})/2$ and the enthalpy is $h = e + p/\rho$. The internal energy for a calorically perfect gas is $e = 5/2\,RT$. The numerical flux is computed using a characteristic-based, upwind scheme.

The viscous flux vector may be written as

$$\mathbf{F}'_v \cdot \hat{\mathbf{n}} = \left\{ \begin{array}{c} 0 \\ \tau'_{xx}\hat{n}_x + \tau'_{xy}\hat{n}_y + \tau'_{xz}\hat{n}_z \\ \tau'_{yx}\hat{n}_x + \tau'_{yy}\hat{n}_y + \tau'_{yz}\hat{n}_z \\ \tau'_{zx}\hat{n}_x + \tau'_{zy}\hat{n}_y + \tau'_{zz}\hat{n}_z \\ -(\nabla q)' \cdot \hat{\mathbf{n}} + \tau'_{ik}u_k\hat{n}_{x_i} + \tau_{ik}u'_k\hat{n}_{x_i} \end{array} \right\}. \tag{5.8}$$

Assuming a linear stress-strain relationship, the viscous shear can be written as $\tau_{ij} = 2\mu\,(S_{ij} - 1/3\,u_{k,k}\,\delta_{ij})$ where S_{ij} represents the strain rate. The sensitivity of the shear-stress tensor is derived by differentiation

$$\tau'_{ij} = 2\mu' \left[S_{ij} - \frac{1}{3}(\nabla \cdot \vec{\mathbf{V}})\delta_{ij} \right] + 2\mu \left[S'_{ij} - \frac{1}{3}(\nabla \cdot \vec{\mathbf{V}}')\delta_{ij} \right], \tag{5.9}$$

where the sensitivity strain rate is

$$S'_{ij} = \frac{1}{2}\left(\frac{\partial u'_i}{\partial x_j} + \frac{\partial u'_j}{\partial x_i} \right).$$

The sensitivity of the conduction term is $(\vec{q})' = -k'\,\nabla T - k\,\nabla T'$.

5.1.6 Boundary Condition Sensitivity

Since our parameters do not explicitly enter the flux terms in Eqn. (5.2), the resulting sensitivity equation Eqn. (5.6) is homogeneous. All the action then is in the boundary conditions and in their explicit dependence on the problem parameters.

In-Flow Condition

Our model is expressed in a coordinate system translating with the vehicle so that the relative fluid velocity is given by the usual Gallilean transformation

$$\vec{\mathbf{V}} = \vec{\mathbf{V}}_{\text{abs}} - \vec{\mathbf{V}}_c.$$

In the present case all of the fluid at the in-flow boundary is at rest, so that we have the inflow conditions:

$$\vec{\mathbf{V}}(x_i) = -\|\vec{\mathbf{V}}_c\| \left[\begin{array}{c} \cos\beta\cos\alpha \\ \sin\beta \\ \cos\beta\sin\alpha \end{array} \right]_h.$$

The in-flow boundary condition for the α-sensitivity is accordingly

$$\left.\frac{\partial \mathbf{q}}{\partial \alpha}\right|_\infty = \|\vec{\mathbf{V}}_c\| \left\{ \begin{array}{c} 0 \\ \cos\beta\sin\alpha \\ 0 \\ -\cos\beta\cos\alpha \\ 0 \end{array} \right\}, \tag{5.10}$$

while for the β-sensitivity we have:

$$\left.\frac{\partial \mathbf{q}}{\partial \beta}\right|_{\infty} = \|\vec{\mathbf{V}}_c\| \begin{Bmatrix} 0 \\ \sin\beta\cos\alpha \\ -\cos\beta \\ \sin\beta\sin\alpha \\ 0 \end{Bmatrix}. \tag{5.11}$$

No-Penetration Condition

Another of the important boundary conditions in Euler flows is the so-called no penetration condition (5.3), now written as $\vec{\mathbf{V}} \cdot \hat{n} = 0$ on the solid boundary. Using the notation introduced above we can write this more precisely as

$$\vec{\mathbf{V}}(\pi(\sigma,\eta);\eta) \cdot \hat{n}(\sigma,\eta) = 0 \quad \forall \sigma \in \Sigma_b. \tag{5.12}$$

Since (5.12) must hold for all η in some open region, Ω_η, we can formally differentiate with respect to η. Note that the flow velocity function is defined over the flow region, that is $\vec{\mathbf{V}} : O \times \Omega_\eta \mapsto R^3$, where $O \subset R^3$ is the flow region. In computing the η-derivative of (5.12) one must be careful to account for the chain-rule terms. This leads to

$$\left(\frac{\partial \vec{\mathbf{V}}}{\partial x}\frac{\partial \pi}{\partial \eta} + \frac{\partial \vec{\mathbf{V}}}{\partial \eta}\right) \cdot \hat{n} + \vec{\mathbf{V}} \cdot \left(\frac{\partial \hat{n}}{\partial \eta}\right) = 0.$$

The velocity sensitivity we seek is captured in the $(\frac{\partial \vec{\mathbf{V}}}{\partial \eta})$ term so that we are led to define

$$\hat{\mathbf{S}} \equiv \frac{\partial \vec{\mathbf{V}}}{\partial \eta}.$$

This is the sensitivity variable we are seeking and the boundary condition on $\hat{\mathbf{S}}$ that arises from the flow-tangency condition is

$$\hat{\mathbf{S}} \cdot \hat{n} = -\left[\frac{\partial \vec{\mathbf{V}}}{\partial x}\frac{\partial \pi}{\partial \eta} \cdot \hat{n} + \vec{\mathbf{V}} \cdot \left(\frac{\partial \hat{n}}{\partial \eta}\right) = 0.\right]. \tag{5.13}$$

The right-side of the boundary condition Eqn. (5.13) can be interpreted as a transpiration condition for the sensitivity. As noted above, the *state* of the fluid in terms of primitive flow variables at a given point in space is given by five quantities $\mathbf{q} = [\rho\ u\ v\ w\ p]^T$ In equation (5.13) we are describing the sensitivity of the *velocity* components. Thus, if we wish to use $\mathbf{S}$ to denote the five-component state-sensitivity there is a 3×5 matrix projection introduced. The left side of (5.13) can be written as:

$$M\mathbf{S} \cdot \hat{n} = \ldots \quad \text{or equivalently} \quad \mathbf{S} \cdot (M^T\hat{n}) = \ldots$$

The particular parameters of interest in the present case are the angle-of-attack α and the side-slip angle β.

Additional Solid Boundary Conditions

Beyond the in-flow and flow-tangency conditions it is common to introduce additional boundary-conditions at solid interfaces in Euler flows. In the present case we shall use three additional (scalar) conditions. Each of these is written in a standard form as

$$\nabla_x \left[f(q(x;\eta)) \right] \cdot \tilde{n}(x,\eta) = 0 \quad \forall\, x \in \Gamma \tag{5.14}$$

where Γ denotes the boundary points. In our application we propose to use the following three scalar-valued functions for f.

1. $f_1(q) = q_1 = \rho$ density
2. $f_2(q) = q_5 = p$ pressure
3. $f_3() = ({q_2}^2 + {q_3}^2 + {q_4}^2)/2$ kinetic energy

Note that the scalar-functions (f) are not explicitly functions of the design-parameter (η). We exploit this to expand (5.14) as

$$\left(\frac{\partial f}{\partial q} \right) \nabla_x q(\pi(\sigma;\eta);\eta) \cdot \hat{n}(\sigma,\eta) = 0 \quad \forall\, \sigma \in \Sigma_b.$$

Recall that points on the boundary are images of the map π. The η derivative of this leads to

$$\left(\frac{\partial f}{\partial q} \right) \nabla_x \mathbf{S} \cdot \hat{n} = - \left(\frac{\partial f}{\partial q} \right) \left[(\nabla_{xx}\, q) \pi_\eta \cdot \hat{n} + \nabla_x q \cdot \hat{n}_\eta \right]. \tag{5.15}$$

The first of the forcing-terms on the right generally involves the *Hessian* of the primitive variables. However, for the present application with $\eta \equiv \alpha$ or β we have that both π_η and $\hat{n}_\eta$ vanish, so that in our applications the b.c. (5.15) are homogeneous.

5.1.7 Applications

As a first numerical example of the SEM approach to estimating stability derivatives, we consider the calculation of the lift-curve slope for a 2-D viscous, compressible flow around an airfoil. A potential benefit for design engineers is the ability to determine the lift-curve slope using a single non-linear flow solution. Specifically, we model the flow around a NLF(1)-0416 airfoil developed at NASA Langley by Somers. The flow conditions ($M_\infty = 0.5$, $Re = 2 \times 10^6$) are extracted from an AGARD set of test cases for validating CFD codes. The pressure contours and streamlines at $\alpha = 0°$ are shown in Fig. 5.1 on a $185 \times 97 \times 2$ "C" mesh.

To proceed in the analysis, we wish determine the sensitivity of the airfoil's lift to the angle of attack. The far-field boundary condition for the SEM is determined by writing the free-stream velocity as a function of the magnitude and angle of attack. In the absence of side-slip, we apply Eqn. (5.10) as our free-stream sensitivity vector with $\beta = 0°$.

Using this free-stream boundary condition, the solution to the sensitivity equations at $\alpha = 0°$ is shown in the following figure. Sensitivity pressure contours and streamlines of velocity-vector sensitivity are depicted. From the pressure sensitivity near the nose, we see that an increase in the angle of attack will cause an increase in the lower-surface pressure and a decrease in the upper-surface pressure. The streamlines show that the magnitude of

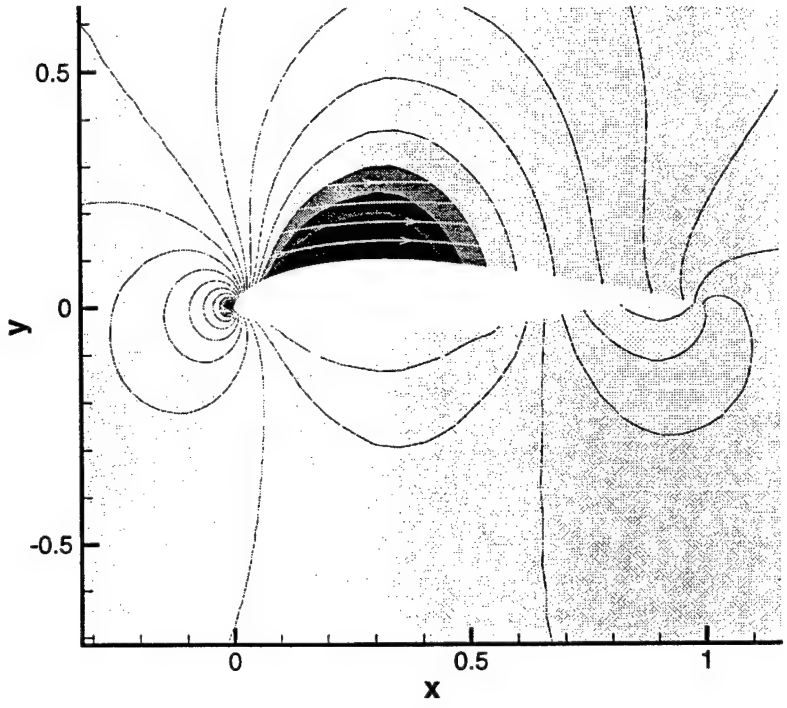

Figure 5.1: Pressure contours and velocity vectors for the NLF(1)-0416 airfoil at zero angle of attack.

the velocity vector will decrease beneath the airfoil surface and increase along the upper surface. Careful investigation at the trailing edge shows that the momentum of the boundary layer is predicted to decrease. All these indications are consistent with an increase in the angle of attack for attached flow. The pressure coefficient and sensitivity are given in FigFig:NLF4$_1$3.

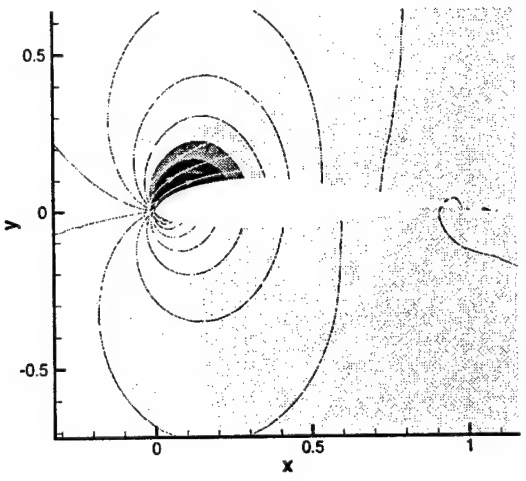

Figure 5.2: Pressure sensitivity and streamlines

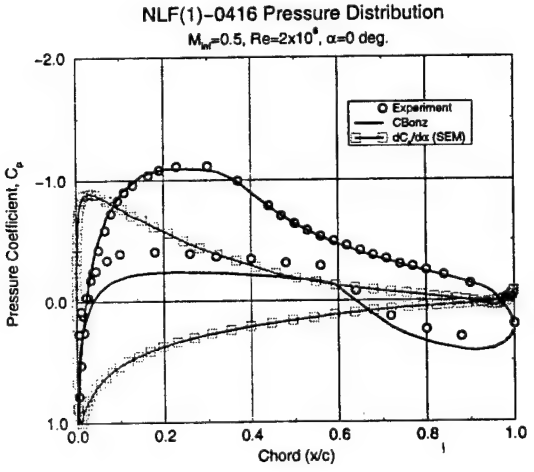

Figure 5.3: Pressure coefficient and sensitivity

To determine the accuracy of the sensitivity method (more fundamentally, the linearity of the local flow condition), we extrapolate the baseline flow to $\alpha = 4°$ using a Taylor-series

expansion

$$\mathbf{Q} = \mathbf{Q}^{(b)} + \left.\frac{\partial \mathbf{Q}}{\partial \alpha}\right|^{(b)} \Delta\alpha. \tag{5.16}$$

The pressure and streamlines for the near-by approximation is given in Fig. 5.4. The predominant flow features are a rearward movement of the stagnation point at the nose and decreased pressure along the upper surface. Notice that the streamlines do not indicate separated flow. The accuracy of the pressure coefficient on the airfoil surface can be evaluated using Fig. ??.

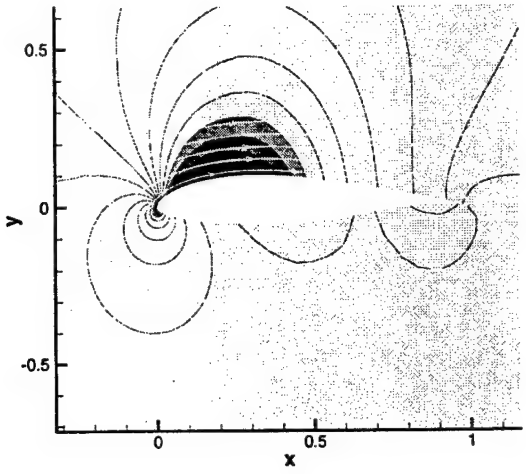

Figure 5.4: Projected solution at $\alpha = 4°$

Performing a sensitivity analysis at $\alpha = 4°$ produces the contour solution shown in Fig. 5.6. The bubbles in the upper-surface pressure sensitivity indicate the beginning and ending of a laminar separation bubble followed by aerodynamic stall. The sensitivity streamlines depict similar behavior to the zero-degree case beneath the airfoil. However, the prediction for the flow above the airfoil is for further flow separation. This is seen by the upward movement of the sensitivity streamlines. Assuming laminar flow over the entire airfoil surface, the computational solution begins to separate at $\alpha = 5°$, consistent with the sensitivity calculation.

The surface pressure coefficient and sensitivity at $\alpha = 4°$ is shown in Fig. 5.7. The sensitivity profile is much different than the smooth variation from nose to tail shown at $\alpha = 0°$. The sensitivity further indicates the likelihood of separated flow at higher angles of attack. The Taylor approximation at $\alpha = 8°$ shows a pressure plateau on the upper surface which indicates the presence of a laminar separation bubble.

Our objective of determining the lift-curve slope from one flow calculation and one sensitivity calculation can be achieved by differentiating the lift coefficient with respect to the angle of attack. Writing the lift coefficient in terms of force coefficients in the x and y

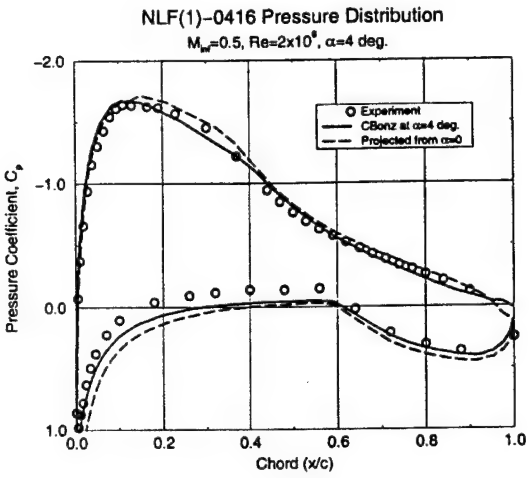

Figure 5.5: Surface pressure coefficient

direction, we have

$$C_l = C_y \cos\alpha - C_x \sin\alpha,$$

so that the lift-curve slope is computed as

$$\frac{\partial C_l}{\partial \alpha} = \left(\frac{\partial C_y}{\partial \alpha}\cos\alpha - \frac{\partial C_x}{\partial \alpha}\sin\alpha\right) - (C_y \sin\alpha + C_x \cos\alpha) \tag{5.17}$$

The sensitivity of the two force coefficients is obtained by integrating the inviscid and viscous fluxes on the airfoil surface. The lift-curve slope is shown in Fig. 5.8 using experiment, computation and sensitivity calculations. The computational lift-curve slope shows more lift at the same angle of attack when compared to experiment. The CFD predicts a higher pressure on the lower surface, thus producing more lift. The sensitivity lift-curve slope is given at $\alpha = 0°$ and $4°$.

5.1.8 Flying-Wing Stability Analysis

As early as 1923, Jack Northrop began advocating the flying-wing concept as the next revolution in aircraft design. In the late 1930's the Northrop Corporation undertook the development of a series of all-wing concepts; and in late 1941 received an order for two propeller-driven flying wings in support of the long-range bombing requirements of the U.S. Army Air Corps. These XB-35's were plagued with both maintenance and accident difficulties. With the growth of the jet-age, the XB-35 airframe was updated with eight Allison J35-A-5 turbo-jets under a contract issued in June, 1945. The new aircraft was designated the YB-49 and a schematic of the flying-wing bomber is shown in Fig. 5.9. Airframe parameters for the plane are given in Table 1.

The perceived advantages of the flying wing were increased aerodynamic efficiency from reduced parasite drag, simpler construction methods from fewer structural complications, and increased stealth from a smaller visual target. Unfortunately, the technology of the day

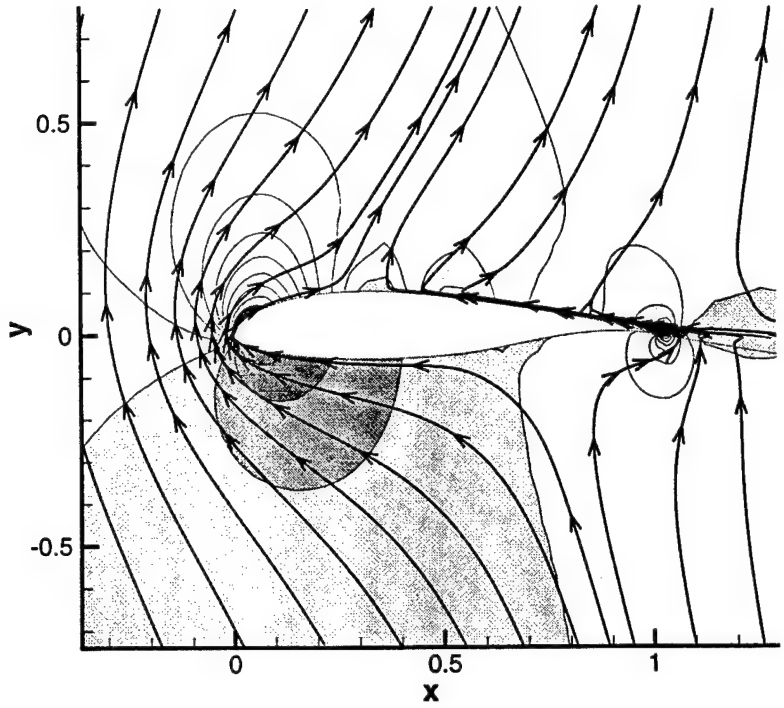

Figure 5.6: Sensitivity of the pressure and velocity vectors to the angle of attack at $\alpha = 4°$. Assuming totally laminar flow, the airfoil begins to stall at $\alpha = 5°$.

could not solve problems associated with the aircraft's stability characteristics – namely, difficulty holding a steady course and altitude, as well as poor damping in yaw. The fly-by-wire concept alleviates some of these problems in the B-2 stealth bomber.

In this section, we will use the sensitivity-equation method to estimate some of the stability characteristics of the YB-49 flying wing. To simplify grid generation, we have neglected the bubble canopy, and four vertical-fins/wing-fences that are a part of the actual YB-49. Our calculations sample the angle-of-attack range ($\alpha = 0°, 4°, 8°$) and we compute C_{L_α}, C_{M_α}, C_{n_β} and C_{l_β} derivatives. The free-stream conditions correspond approximately to cruise speed ($M_\infty = 0.5$) at an altitude of 35,000 feet.

Pitch Stability

Stability in pitch requires, of course, that in the neighborhood of an equilibrium point the slope of the pitch moment with angle-of-attack be negative. This leads to the stipulation that the center-of-gravity be suitably forward of the mean aerodynamic center – defined, loosely, as the point about which the moment-slope is zero.

For an inviscid-flow CFD model, the pitching moment is computed as an appropriate

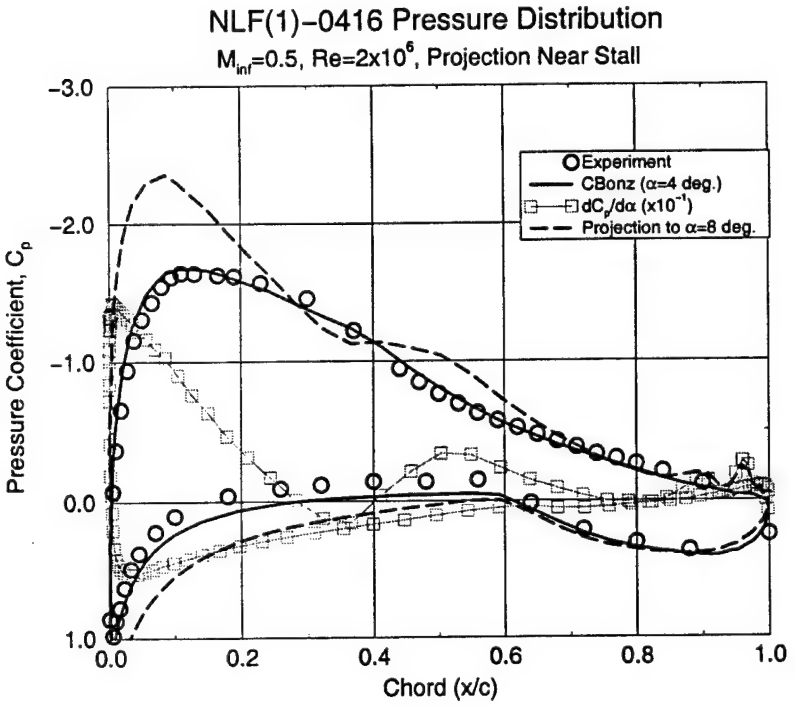

Figure 5.7: Surface pressure coefficient at $\alpha = 4°$ and $8°$ along with the pressure sensitivity.

surface integral of the normal pressure. We write this as an iterated integral

$$M(\alpha) = \int_{-b/2}^{b/2} \left[\oint_{C(y)} p(x, y, z; \alpha)\, d(\frac{x^2 + z^2}{2}) \right] dy. \tag{5.18}$$

The inner term is identified as a familiar section contour integral and represents the contribution to the pitching moment at spanwise location y. One may plot this *pitch-loading* against the spanwise location y as shown in Fig. 5.10.

In the present treatment the longitudinal stability parameter M_α is evaluated in the same way with the pressure replaced by the pressure sensitivity p_α. One may describe the inner integral as the *stability loading* function; it describes the contribution to pitch stability from various locations along the wing-span. Fig. 5.11 displays the stability loading for the YB-49 planform at $\alpha = 4°$ and $\alpha = 8°$. While the result is not dramatic, one can clearly see the decrement in the stability contribution from the outboard wing panels. This feature was described qualitatively by J. Northrop in his 1947 Wilbur Wright Memorial Lecture.

Contours of the pressure sensitivity to the angle of attack are shown in Fig. 5.12 and Fig. 5.13. The domain is composed of ten zones composed of approximately 620,000 grid points. Both the Euler equations and the sensitivity equations are solved using a first-order spatially accurate flux-vector splitting scheme. The residual for the Euler equations are converged four orders of magnitude in approximately 2250 iterations. The sensitivity equations exhibit some stiffness for these calculations that has not been experienced in

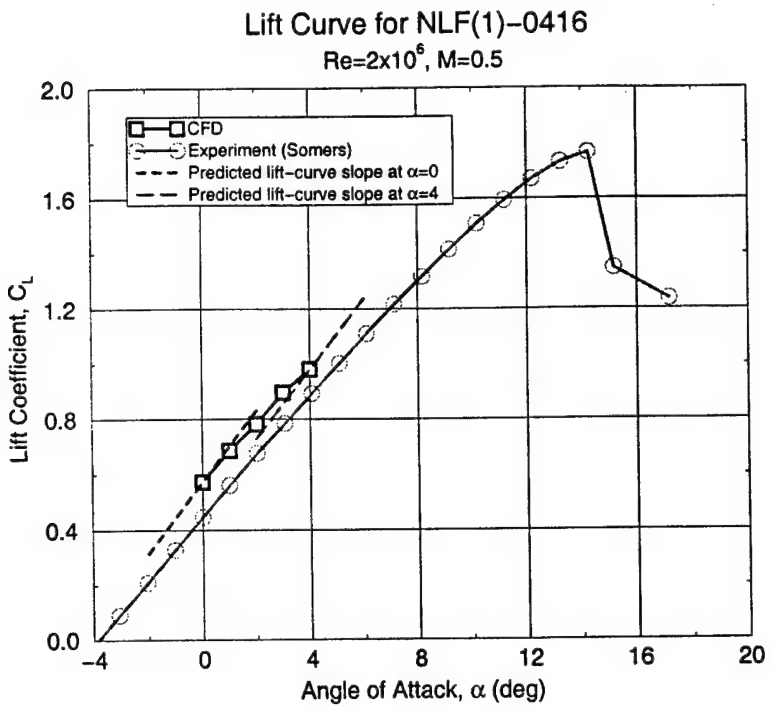

Figure 5.8: Lift-curve slopes obtained from experiment, CFD flow solver and the sensitivity-equation method.

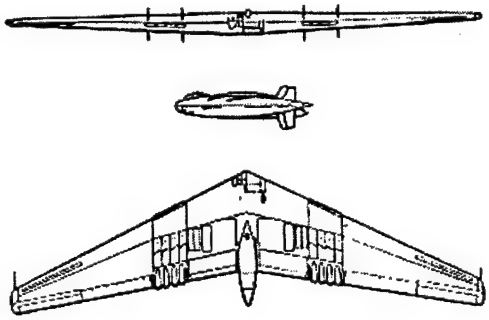

Figure 5.9: Three-view schematic of the YB-49 flying wing.

past SEM calculations. The theoretical reasons for this have not been investigated. In general, the sensitivity equations, being linear, can be solved using an infinite time step. A smaller time step is used for the $\eta = \alpha$, β cases for two reasons: the fore-mentioned stiffness and also because the problem is three-dimensional which requires a compromise between convergence and memory. A hybrid Euler implicit/relaxation scheme is used to sweep

Wing span (b)	52.4 m
Wing area (S)	371.6 m^2
Aspect ratio (A)	7.4
Taper ratio (λ)	0.25
Chord	11.4 m (Root)
	2.8 m (Tip)
Airfoil section	NACA $65_3 - 018$ (Root)
	NACA $65_3 - 019$ (Tip)
Incidence	$0°$ (Root)
	$-4°$ (Tip)
Dihedral	$0°53'$
Sweep	$26°57'48"$ (LE)
	$10°15'22"$ (TE)
M.A.C.	8 m (7.33 m aft of nose)
C.G.	7.13 m aft of the nose (est.)
Ceiling	45,700 feet
Cruising speed	429 mph at 35,000 feet

Table 1: Airframe data for the YB-49 configuration.

through the domain. Updates to the sensitivity vector are computed on two-dimensional "planes" (in computational space) using Jacobi inner iterations with non-linear residual updates computed in the third direction. Therefore, a complete linearization of the SEM residual requires storage of the entire linearization matrix for all computational planes and all zones which is impractical with limited memory. The compromise made for saving memory is diminished convergence rate. The sensitivity calculations require an average of 60 iterations to converge – about 2.7% of the time to compute the flow solution. The SEM equations requires more memory than the Euler solutions because both the flow variables ($\mathbf{Q}$) and sensitivity variables ($\mathbf{Q}'$) are retained in memory during the calculation.

The performance of the wing's lift and moment are summarized in Table 2 and Table 3, respectively. A comparison is made with a standard semi-empirical formula for the lift-curve slope which corrects the two-dimensional airfoil C_{l_α} for taper ratio, sweep angle, aspect ratio and Mach number. Using the airfoil data, we estimate the section lift-curve slope as $C_{l_\alpha} = 6.0877/\text{rad}$ for a NACA $65_3 - 018$. Mach effects are introduced based on the free-stream Mach number for the calculation, *i.e.*, $M_\infty = 0.5$. The maximum thickness of the airfoil occurs at $x/c = 40\%$, which gives a sweep angle of $\Lambda_{\text{max t}} = 20.7562°$.

The MAC/C.G. data is used to compute the moment slope via $C_{M_\alpha} = -C_{L_\alpha} h_n$. Note that the center of gravity is estimated using relationships between the center of gravity and the location of aircraft landing gear. Namely, we assume the landing gear is located 15° aft of the center of gravity. The finite-difference values in the tables are computed using the $\alpha = 0°$ and $\alpha = 8°$ Euler solutions. An argument could be made that these numbers should be computed using an epsilon change in the angle of attack.

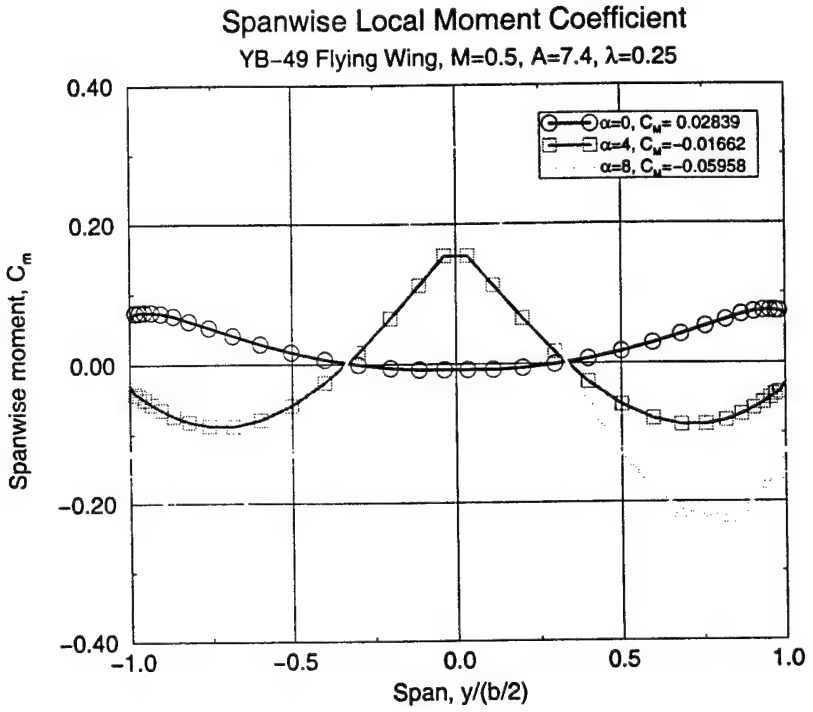

Figure 5.10: Spanwise moment distribution along the wing.

	C_{L_α}		
α	Raymer	Fin. Diff.	SEM
0°	—	—	4.3089
4°	4.2997	5.0715	4.0818
8°	—	—	4.0424

Table 2: Comparison of lift-curve slope between semi-empirical, finite-difference and sensitivity-equation method.

5.1.9 Lateral/Directional Stability

Lateral/Directional Stability

Some data on XB-35 lateral/directional stability is presented in Northrop in his Wright Memorial Lecture to the RAE. For this pusher-propeller configuration a considerable amount of weathercock stability is provided by the engine-drive nacelles, as well as the propellers themselves. Since our model does not include these features, it is expected that the bare-wing estimate for C_{n_β} will be smaller than Northrop's data.

The sensitivity of the wing pressure to the sideslip angle is shown in Fig. 5.14 and Fig. 5.15. The pressure sensitivity on the upper surface of the right wing is negative leading to an addition to the local lift. The opposite occurs for the left wing where pressure

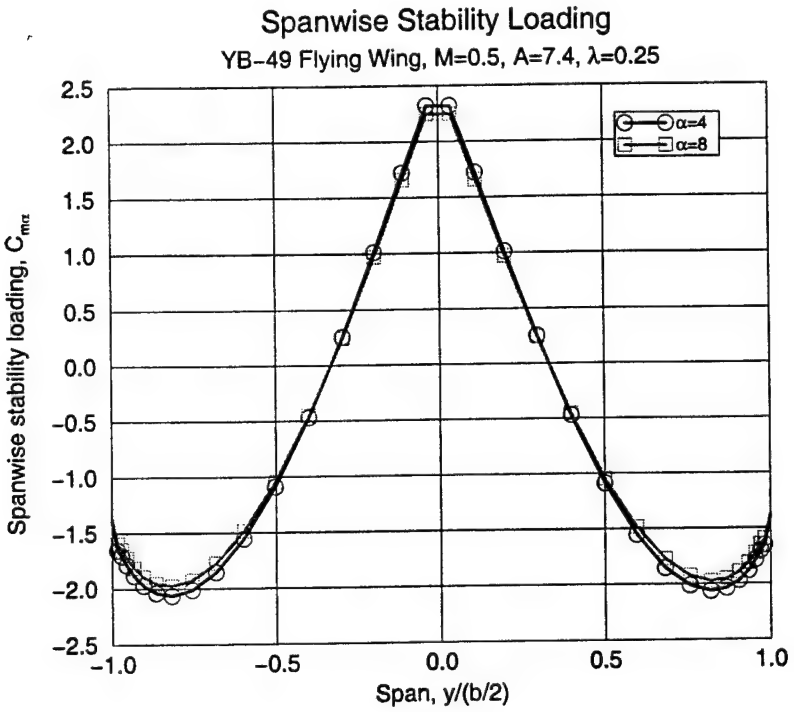

Figure 5.11: Spanwise stability loading distribution along the wing.

	C_{M_α}		
α	Raymer	Fin. Diff.	SEM
0°	—	—	−0.4613
4°	-0.4743	−0.6301	−0.4344
8°	—	—	−0.4450

Table 3: Comparison of pitching-moment stability between semi-empirical, finite-difference and sensitivity-equation method.

sensitivities are positive resulting in less lift. The lift differential leads to rolling/yawing moment.

A comparison between Northrop's data, finite difference and the sensitivity-equation method is given in Table 4 and Table 5 for the rolling and yawing rate derivatives, respectively. These are sometimes called the effective dihedral and the weathercock stability derivatives. The trends in the stability derivatives are consistent with Northrop's data as the angle of attack increases. As expected, the weathercock stability is less than the actual aircraft which uses vertical fins for increased yaw stability.

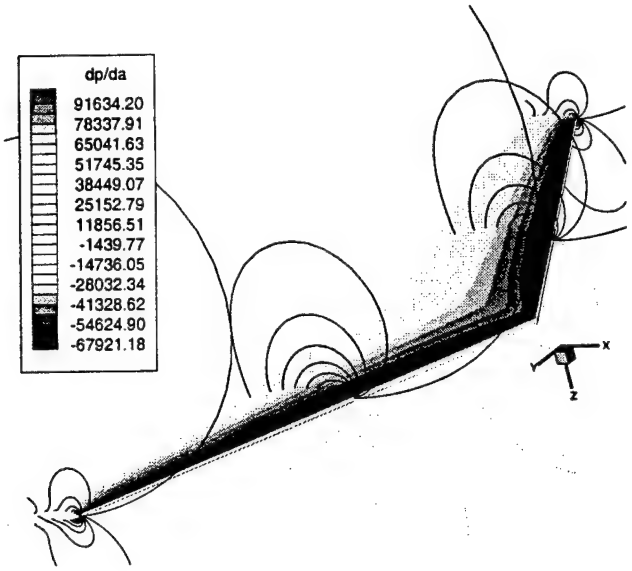

Figure 5.12: Upper surface

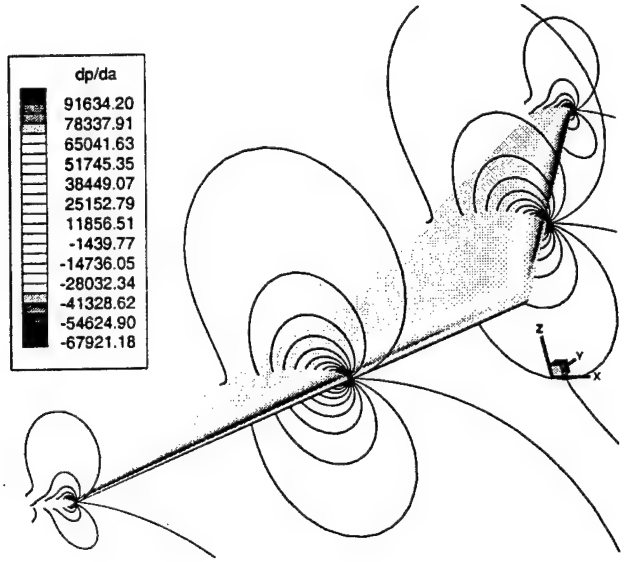

Figure 5.13: Lower surface

5.1.10 Summary

The sensitivity equation method (SEM), applied to nonlinear flow analyses, produces a linear boundary-value problem. The solution to this problem is a *flow sensitivity* and describes, in linear approximation, the dependence of the flow-solution on a scalar parameter. The derivative of any non-linear functional of the flow with respect to this parameter can be

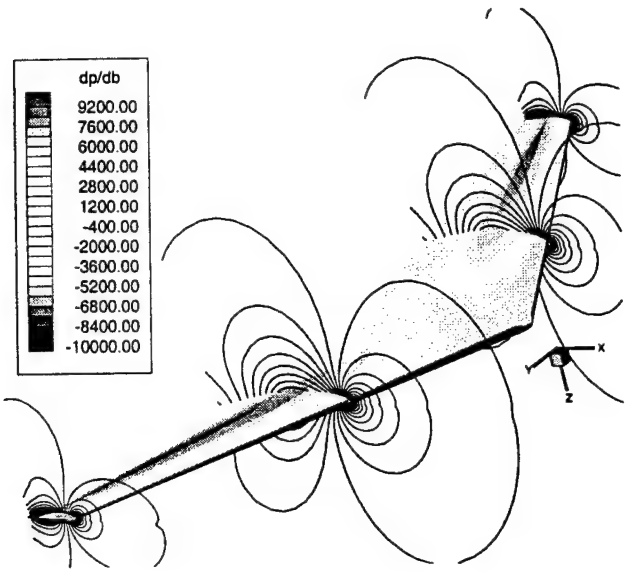

Figure 5.14: Upper surface

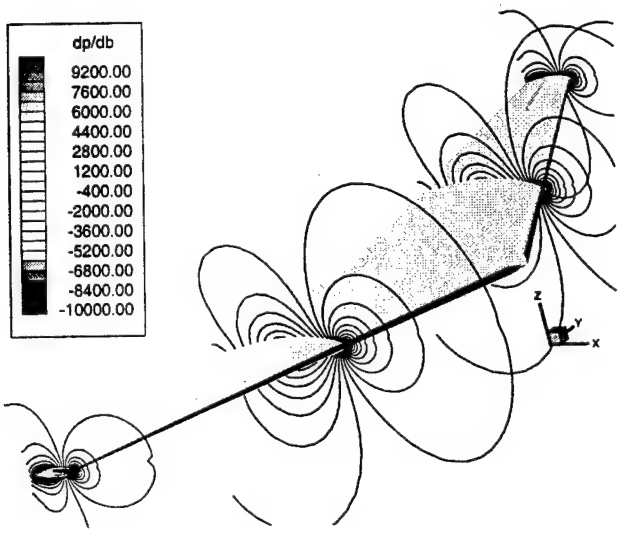

Figure 5.15: Lower surface

easily computed from the chain rule. This latter calculation requires evaluation of a single inner product so the computational effort is negligible.

While the SEM has a number of applications, in the present case we have applied the method to the calculation of force and moment stability derivatives. The SEM is computationally efficient; after calculation of the underlying flow, the linear boundary-value problem is typically solved in 3% of the time required for a non-linear flow solution.

	C_{l_β}		
α	Northrop	Fin. Diff.	SEM
4°	−0.029	−0.0347	−0.0318
8°	−0.057	−0.0696	−0.0667

Table 4: Computed effective-dihedral stability derivatives.

	C_{n_β}		
α	Northrop	Fin. Diff.	SEM
4°	0.020	0.0159	0.0142
8°	0.026	0.0215	0.0203

Table 5: Computed weathercock stability derivatives.

A single sensitivity can be used to calculate the derivative of a number of force/moment functionals (*e.g.*, $C_{n\beta}$, $C_{\ell\beta}, C_{y\beta}$).

Stability derivatives for asymmetric flight can be calculated based on a symmetric flow solution so that configuration symmetry can be exploited. The method naturally extends to calculation of control derivatives, body-rate derivatives and aeroelastic derivatives.

5.2 The Impact of Finite precision Arithmetic on Sensitivity

In this section we address some fundamental issues concerning "time marching" numerical schemes for computing steady state solutions of boundary value problems for nonlinear partial differential equations. Simple examples are used to illustrate that even theoretically convergent schemes can produce numerical steady state solutions that do not correspond to steady state solutions of the boundary value problem. This phenomenon must be considered in any computational study of non-unique solutions to partial differential equations that govern physical systems such as fluid flows. In particular, numerical calculations have been used to "suggest" that certain Euler equations do not have a unique solution. For Burgers' equation on a finite spatial interval with Neumann boundary conditions the only steady state solutions are constant (in space) functions. Moreover, according to recent theoretical results, for any initial condition the corresponding solution to Burgers' equation must converge to a constant as $t \to \infty$. However, we present a convergent finite difference scheme that produces false nonconstant numerical steady state "solutions." These erroneous solutions arise out of the necessary finite floating point arithmetic inherent in every digital computer. We suggest the resulting numerical steady state solution may be viewed as a solution to a "nearby" boundary value problem with high sensitivity to changes in the boundary conditions. Finally, we close with some comments on the relevance of this paper to some recent "numerical based proofs" of the existence of non-unique solutions to Euler equations and to aerodynamic design.

5.2.1 Introduction and Motivation

During the past twenty years there have been a significant advances in computational tools for optimal design and control of fluid flows. Many of these tools are based on cascading simulation software into optimization and/or control schemes. Although this method has been applied to some complex aerodynamic control problems, very little has been done to develop a rigorous theory of convergence for the resulting optimal design and control algorithms. Even if the partial differential equation that defines the relationship between state and control variables has a unique solution for each control, numerical approximations may not preserve this uniqueness. In particular, the discretized state equations may yield "false" non-unique solutions which may drive the optimization algorithm to an incorrect design. As a first step in understanding when and why a particular algorithm converges to an optimal design for the governing partial differential equations, it is essential to know when and why these extraneous numerical solutions occur.

Herewe focus on just such an issue. In particular, we use a simple Neumann boundary value problem for the one dimensional Burgers' equation to illustrate that, because of finite precision arithmetic, a convergent numerical algorithm can produce false (purely numerical) solutions. The main purpose of this work is to give an in-depth examination of this model problem and to give warning in the use of numerical based proofs of uniqueness for hydrodynamic problems.

The problem discussed in this paper is caused by computing on a finite precision machine and is not caused by roundoff errors. Also, the issue considered here is not the same as supersensitivity considered by other authors.

In 1993 Marrekchi, while working on a Neumann boundary control problem for Burgers' equation, observed that a finite element scheme used to design feedback controllers produced non-constant steady state solutions. It is now known that these "solutions" are purely numerical and, as we show below, most numerical methods will generate such false solutions. If a boundary value problem as simple as Burgers' equation with Neumann conditions can lead to such complex phenomena, then it is reasonable to expect similar difficulties for potential and Euler type equations.

Before turning to Burgers' equation, we present a simple example that illustrates the basic difficulty.

Example 1 Let $\alpha \geq 0$ and consider the initial value problem

$$\begin{cases} \dfrac{dy}{dx} = g(y,\alpha) \\ \\ y(0) = 1 \end{cases} \quad \text{where} \quad g(y,\alpha) = \begin{cases} \alpha & \text{if } y(x) \leq 1 + 10\alpha \\ \\ 1 & \text{if } y(x) > 1 + 10\alpha \end{cases}.$$

The exact solution to this problem is given by

$$y(x) = \begin{cases} 1 + \alpha x & , \quad 0 \leq x \leq 10 \\ \\ 1 + 10\alpha + (x - 10) & , \quad x \geq 10 \end{cases}.$$

However, if we apply a standard numerical method, such as Euler's method, to this problem we see something very different because of the use of finite precision arithmetic. Namely,

let Δx be a small increment, define $x_j = j\Delta x$ and $y_j \sim y(x_j)$. Then the Euler iterates are given by

$$y_{j+1} = y_j + g(y_j, \alpha)\Delta x, \quad y_0 = 1,$$

and for $j = 0$,

$$y_1 = y_0 + g(y_0, \alpha)\Delta x = 1 + \alpha\Delta x.$$

Now for $\alpha\Delta x$ sufficiently small and with finite precision arithmetic, $y_1 = y_0 = 1$, i.e., if $\alpha\Delta x$ is smaller than $(1/2)2^{1-d}$ where d is the number of digits (assuming base 2 arithmetic), then $1 + \alpha\Delta x = 1$. (Note: the smallest positive number can be different than unit rounding error (machine precision).) Thus, the numerical solution to this problem gives

$$y_j = 1, \quad \text{for all } \ j \geq 0.$$

As an example, on a particular desktop computer using MATLAB, the machine precision is given in a variable denoted by *eps* whose value, for this machine, is $eps = 2.2204460492503131\,0^{-16}$ satisfying

$$1 + eps = 1.0000000.$$

As a numerical experiment set $\Delta x = .005$ and successively solve the above initial value problem using Euler's method as described above with a sequence of decreasing values $\alpha = 10^{-j}$ $j = 1, \cdots, 14$. For all $j \leq 12$ the sequence of iterates give the approximation to the correct solution but when $j = 14$ the iterates give $y_j = 1$. We note that in this case

$$\Delta x \times 10^{-14} = 5 \times 10^{-17} < eps < \Delta x \times 10^{-12} = 5 \times 10^{-15}.$$

The solutions for these cases are depicted in Figure 1. The lines depict numerical solutions for $\alpha = 10^{-14}$ and $\alpha = 10^{-12}$.

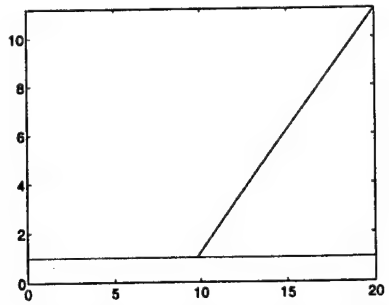

FIG. 1. Machine Floating Point Problem

It is important to note that mesh refinement only exacerbates the matter. For example, if $\alpha = 10^{-12}$ and Δx is reduced to $\Delta x = 5 \times 10^{-5}$, then $\Delta x \times 10^{-12} = 5 \times 10^{-17} < eps$. Therefore, once again the numerical solution $y_i = 1$ will be incorrect. On the other hand, for $\alpha = 0$ the solution to

$$\begin{cases} \dfrac{dy}{dx} = g(y, 0) \\ y(0) = 1 \end{cases} \quad \text{where } \ g(y,0) = \begin{cases} 0 & \text{if } \ y(x) \leq 1 \\ 1 & \text{if } \ y(x) > 1 \end{cases},$$

is given by $y(x) \equiv 1$, and hence the numerical solution for $10^{-12} = \alpha > 0$ is "correct" for the problem defined by $\alpha = 0$. We suggest that some of the numerical problems considered below for Burgers' equation follows a similar pattern.

Burgers' equation on the interval $(0,1)$ subject to Neumann Boundary Conditions is given by the dynamical system

$$\begin{aligned} & w_t - \epsilon w_{xx} + w w_x = 0, \\ & x \in (0,1), \quad t > 0, \ \epsilon > 0, \\ & w_x(0,t) = w_x(1,t) = 0, \\ & w(x,0) = \phi(x). \end{aligned} \tag{5.19}$$

We are interested in the corresponding steady state problem

$$\begin{aligned} & -\epsilon v_{xx}(x) + v(x) v_x(x) = 0, \\ & v_x(0) = v_x(1) = 0. \end{aligned} \tag{5.20}$$

Solutions of (5.20) are called *stationary* (or equilibrium) solutions of the unsteady problem (5.19). One approach to the development of numerical methods for solving (5.20) is to solve the time dependent problem (5.19) and assume that $w(\cdot,t) \to v(\cdot)$ as $t \to +\infty$. In order to construct fast and accurate "time marching" schemes based on this idea, a number of points must be considered. In particular, one should address the following issues.

(a) If possible, the questions of existence and uniqueness of stationary solutions to the boundary value problem (5.20) needs to be answered. These are still open questions for many fluid and gas dynamic problems.

(b) One needs to know that for reasonable initial data $\phi(\cdot)$, the time varying solution $w(\cdot,t)$ exists for all $t > 0$, $\lim_{t \to +\infty} w(\cdot,t) = v(\cdot)$ exists, and $v(\cdot)$ is a stationary solution.

(c) The rate at which $w(\cdot,t) \to v(\cdot)$ is important because it can influence the efficiency of the scheme.

(d) If one introduces a numerical approximation (with spatial mesh size Δx) and constructs the numerical solution $w^{\Delta x}(\cdot,t)$ with the property that as $\Delta x \to 0$ (i.e. mesh refinement) $w^{\Delta x}(\cdot,t) \to w(\cdot,t)$, then $\lim_{t \to +\infty} w^{\Delta x}(\cdot,t) = v^{\Delta x}(\cdot)$ needs to exist.

(e) The limit $v^{\Delta x}(\cdot)$ is assumed (or proven) to be a good approximation to $v(\cdot)$. This issue is more complicated than one might guess and it can fail in surprisingly simple problems.

Items (a) - (e) above do not address all of the of important issues. For example, as we show in this paper, even if items (a)-(d) are satisfied and one can prove (this means using infinite precision arithmetic) that $v^{\Delta x}(\cdot) \to v(\cdot)$, then problem sensitivity and finite precision arithmetic can produce numerical solutions $v^{\Delta x}(\cdot)$ that do not approximate any stationary solution! Thus, it is possible for a perfectly sound theoretical algorithm to produce "false"

numerical solutions to the steady state problem. We demonstrate this point by a complete analysis of Burgers' equation with Neumann boundary conditions.

In the next section we present the basic analytical results for systems (5.19) and (5.20). We then present some numerical results to illustrate the theoretical results and to demonstrate a numerical anomaly for this problem. The remainder of the paper is devoted to the construction and analysis of numerical schemes so that items (a)-(e) are established and yet numerical solutions generated by these schemes do not approximate the true stationary solutions. We close with a discussion of how the results in this paper may relate to "numerical based proofs" of nonunique stationary solutions for other problems.

5.2.2 Burgers' Equation with Neumann BCs

As pointed out in our earlier work, the linearization about zero of (5.19) in $L^2(0,1)$ is the one dimensional heat equation with Neumann boundary conditions. A well known consequence of the Fourier representation of the solution for this problem shows that the unique steady state response, for any initial data $\phi \in L^2(0,1)$, is the constant function with value equal to the average of the initial data, i.e.,

$$\lim_{t\to\infty} w(x,t) = \int_0^1 \phi(x)\, dx.$$

For Burgers' equation with Neumann boundary conditions it is easy to see that, $w(x,t) = c$ for any $c \in \mathbb{R}$ and all $(x,t) \in (0,1) \times [0,\infty)$ is a stationary solution. A somewhat deeper result for (5.19), can be based on an infinite dimensional version of the Center Manifold Theorem. For sufficiently small initial data in $H^1(0,1)$, the solution $w(x,t)$ of (5.19) tends to a constant as $t \to \infty$. Since the Center Manifold Theorem is a local result it cannot be used to make any general statements about the long time behavior of solutions to (5.19) for larger initial data.

Another possible approach to determining the long time behavior of solutions to (5.19) would consist in determining the existence and properties of a global attractor. Note that since such an attractor must contain all stationary solutions, it must contain all constants, so it must be unbounded.

Actually, a more relevant first question to answer is whether solutions even exist for all time for all initial data $\phi \in L^2(0,1)$, i.e., is there a globally defined dynamical system.

In the 1957 paper by Kiselev and Ladyzenskaya, they prove the global existence and regularity for multi-dimensional Burgers' equation with Dirichlet boundary conditions using a priori estimates and the maximum principle. While this paper is best known for its contributions to Navier-Stokes theory it also has a section devoted to Burgers' equation.

The main facts needed here are listed in the following theorem.

Theorem 5.1 *For the system (5.19) with arbitrary initial data $\phi \in L^2(0,1)$ and $0 < T < \infty$,*

a) There exists a unique globally defined weak solution so that for each $T > 0$

$$w \in C([0,T], L^2(0,1)) \cap L^2([0,T], H^1(0,1)),$$

b) The solution is instantly infinitely smooth (and therefore classical) for $t > 0$.

c) Therefore, there is a globally defined dynamical system on the state space $L^2(0,1)$ given in terms of a nonlinear semigroup $\{T_t, t \geq 0\}$, i.e., the solution is given by $w(x,t) = T_t(\phi)(x)$ for initial data ϕ. This semigroup possesses the following properties:

i) T_t is continuous in t and $\varphi \in L^2(0,1)$.

ii) T_t is compact for $t > 0$.

iii) There exists a positive continuous monotone increasing function $a(\xi)$, $\xi \geq 0$ such that $a(0) = 0$ and

$$\|T_t\varphi\| \leq a(\|\varphi\|),\ t \in [0,\infty),\ \varphi \in L^2(\Omega),$$

which means that the system is globally Lyapunov stable.

iv) There is a global, locally compact attractor $\mathcal{A}$.

In order to see why there must be a global, locally compact attractor we note that by the previous theorem:

1. For every $R > 0$, the ball $B_{a(R)}$ is an absorbing ball for
$$B_R = \{\psi \in L^2(\Omega) : \|\psi\| \leq R\}$$
2. This implies that for every $R > 0$, the dynamical system given by T_t, restricted to $B_{a(R)}$ has a nonempty, compact, connected (local) attractor, which we denote by $\mathcal{A}_R$.
3. It is clear that $R_1 \leq R_2$ implies $\mathcal{A}_{R_1} \subset \mathcal{A}_{R_2}$, and hence we can conclude that $\mathcal{A} = \bigcup_{R \geq 0} \mathcal{A}_R$ is the global attractor.
4. The global attractor $\mathcal{A}$ is only locally compact since $\mathbb{R} \subset \mathcal{A}$.
5. Indeed, for $R > 0$ sufficiently small, the attractor $\mathcal{A}_R$ for the ball $B_R(0)$ consists only of constants (due to the center manifold theorem), i.e.,
$$\mathcal{A} \cap B_R(0) = \mathcal{A}_R = \{c : |c| < a(R)\}.$$

We should comment that since the global attractor contains all stationary solutions and, as we have already mentioned above, every scalar is a stationary solution, the attractor is unbounded. Due to Theorem 2.1 it is locally compact. The exact composition of the attractor has recently been settled by Edriss Titi and Chongsheng Cao.

Theorem 5.2 (Cao and Titi) *For every initial $\phi \in L^2(0,1)$ there is a constant c so that*

$$\sup_{x \in [0,1]} |z(x,t) - c| \xrightarrow{t \to \infty} 0.$$

The dimension of the global attractor is one and consists of the scalars.

For fixed ϵ and for small initial data, numerical approximation of the solutions to (5.19) supports the conclusion of the Center Manifold Theorem and Theorem 5.2. In particular, solutions tend to a constant as t tends to infinity. But for fixed ϵ and "certain" initial data (not too small), some numerical solutions converge to a nonconstant function. These same nonconstant steady state limits are readily obtained using many different numerical algorithms and on various computer platforms. We are led to conjecture the existence of some type of *Numerical Stationary Solutions* for the problem (5.19).

One class of initial data for which this occurs is the "antisymmetric" functions, that is, functions that are odd about $x = 1/2$ in the interval $(0,1)$,

$$L^2_{\rm AS}(0,1) = \left\{\phi \in L^2(0,1) \,:\, \phi(x) = -\phi(1-x)\right\}. \tag{5.21}$$

For initial data $\phi \in L^2_{\rm AS}(0,1)$, a straightforward consequence of Theorem 2.1 is that $w(\cdot,t) \in L^2_{\rm AS}(0,1)$ for all t. This can easily be seen from the uniqueness and the fact that if $\phi \in L^2_{\rm AS}(0,1)$ and $w(x,t)$ is the solution of (5.19), then the function $z(x,t) = -w(1-x,t)$ also satisfies (5.19) and hence

$$w(x,t) = -w(1-x,t)$$

i.e., $w(\cdot,t) \in L^2_{\rm AS}(0,1)$. Note that a continuous function ϕ in $L^2_{\rm AS}(0,1)$ must satisfy $\phi(1/2) = 0$ and so, for $t > 0$ a solution with initial data $\phi \in L^2_{\rm AS}(0,1)$ will satisfy $w(1/2,t) = 0$ for all $t > 0$. These comments establish the following lemma.

Lemma 5.3 *The Hilbert space $L^2_{AS}(0,1)$ is invariant under the nonlinear semigroup T_t (defined in Theorem 5.1 part d)) for the dynamical system (5.19). Thus, for initial data $\phi \in L^2_{AS}(0,1)$,*

$$\lim_{t\to\infty} w(x,t) = 0, \quad \textit{for every} \quad x \in [0,1].$$

Note that a weak stationary solution must satisfy the differential equation

$$\left(-\epsilon v_x + \frac{v^2}{2}\right)_x = 0, \tag{5.22}$$

where all the derivatives are understood as weak derivatives and the equality holds for almost every x. One possibility is that v is a constant, in which case we have,

$$c_0 = \frac{v^2}{2}. \tag{5.23}$$

Clearly a constant provides a stationary solution since, in addition, it satisfies the boundary conditions.

The only distributional solution of the equation

$$\psi'(x) = 0$$

is a constant, so any other stationary solution to (5.19) must satisfy

$$-\epsilon v_x + \frac{v^2}{2} = c_0, \; c_0 \in \mathbb{R}. \tag{5.24}$$

This equation can be solved explicitly with solution given by

$$v(x) = \sqrt{2c_0}\tanh\left(\frac{\sqrt{2c_0}}{2\epsilon}(c_1 - x)\right), \tag{5.25}$$

where c_0 and c_1 are arbitrary constants. A straightforward calculation yields

$$v_x(x) = -\frac{c_0}{\epsilon}\mathrm{sech}^2\left(\frac{\sqrt{2c_0}}{2\epsilon}(c_1 - x)\right), \tag{5.26}$$

and these functions cannot vanish at $x = 0$ or $x = 1$ (unless $c_0 = 0$). Thus, as we already know from Theorem 5.2 the only stationary solutions to Burgers' equation satisfying homogeneous Neumann boundary conditions are constants.

The nonconstant functions $v(\cdot)$ given by (5.25) form a two parameter family depending on the parameters c_0 and c_1. In order that such a function be in $L^2_{\mathrm{AS}}(0,1)$ it follows that $c_1 = 1/2$. We shall focus on functions $h(\cdot) \in L^2_{\mathrm{AS}}(0,1)$ defined by

$$h(x) = \sqrt{2c_0}\tanh\left(\frac{\sqrt{2c_0}}{2\epsilon}(1/2 - x)\right). \tag{5.27}$$

Although $h(\cdot)$ satisfies equation (5.22) exactly, it only approximately satisfies the boundary conditions (to within exponentially small terms). Namely, the functions in (5.27) satisfy (5.22) and

$$h'(x) = -\frac{c_0}{\epsilon}\mathrm{sech}^2\left(\frac{\sqrt{2c_0}}{2\epsilon}(1/2 - x)\right), \tag{5.28}$$

which for small ϵ and/or large c_0 gives

$$h'(0) = h'(1) = -\frac{c_0}{\epsilon}\mathrm{sech}^2\left(\frac{\sqrt{2c_0}}{4\epsilon}\right) = -\alpha, \tag{5.29}$$

where α is an exponentially small positive number.

Thus, if α is close to 0, then the "nearby" steady state problem defined by Burgers' equation

$$-\epsilon v_{xx}(x) + v(x)v_x(x) = 0, \tag{5.30}$$

with (nonhomogeneous) Neumann boundary conditions

$$v_x(0) = v_x(1) = -\alpha, \tag{5.31}$$

will have non-constant solutions $h(\cdot)$ given by (5.27). As we see below, these solutions may appear as the limit (as $t \to +\infty$) of the numerical solutions to the boundary value problem (5.19).

5.2.3 Motivating Numerical Examples

We now provide several examples in order to demonstrate the actual behavior of numerical solutions to (5.19). In all of the simulations given in this section we have set $\epsilon = .1$ and have applied the finite difference method presented below with spatial mesh size $\Delta x = 0.0125 =$

1/80 and temporal mesh size $\Delta t = 0.0004$. We conducted these numerical experiments on varying time intervals and for a variety of initial data. We note that the same results occur for a wide variety of finite element, spectral approximation, and other finite difference schemes.

Observe that the all of the initial data $\phi(\cdot)$ belongs to $L^2_{\mathrm{AS}}(0,1)$ so that, by Lemma 5.3, the solution to (5.19) should approach zero as $t \to +\infty$. Indeed, this is exactly what happens when the initial condition $\phi(\cdot)$ is "small", as illustrated in Figure 1 and Figure 2.

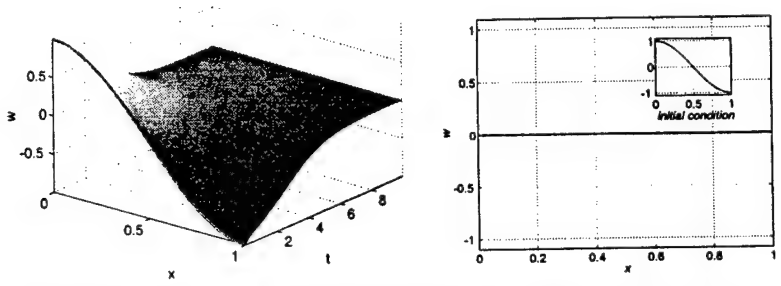

FIG. 2. Initial data $\phi(x) = \cos(\pi x)$ and final time $T = 10$

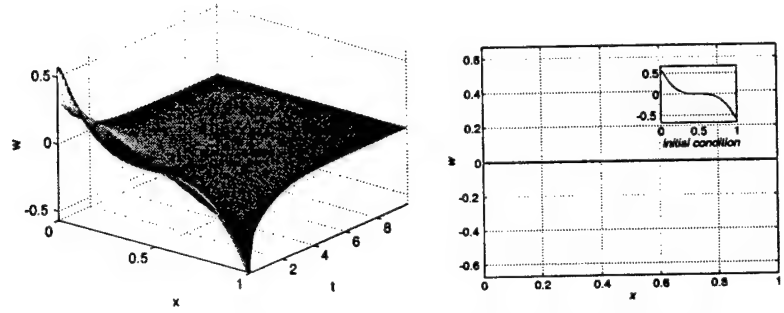

FIG. 3. Initial data $\phi(x) = 5(1/2 - x)^3$ and final time $T = 10$

However, when the amplitude of the initial data is increased we observe that the numerical solutions do not converge to zero. In fact, they appear to converge to a solution of the nearby problem defined by (5.30)-(5.31). More will be said about this phenomenon in the conclusions. In Figure 4 we have increased the amplitude of the cosine function from 1 to 5 and in Figure 5 we have increased the amplitude of the cubic initial function from 5 to 20

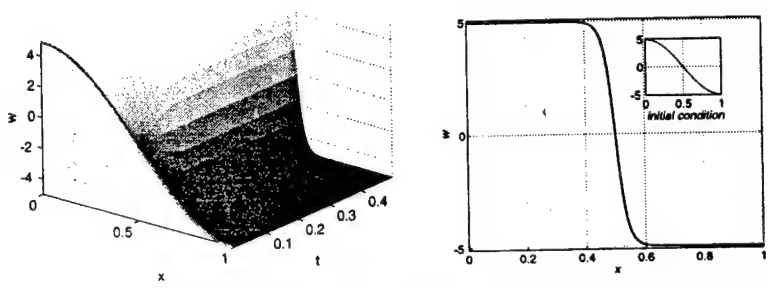

FIG. 4. Initial data $\phi(x) = 5\cos(\pi x)$ and final time $T = 0.25$

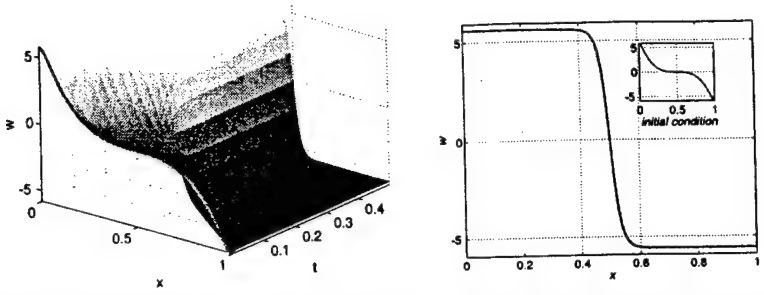

FIG. 5. Initial data $\phi(x) = 50(1/2 - x)^3$ and final time $T = 0.25$

Next we consider an initial condition to show that the same results hold even for initial data that are not strictly decreasing. In particular, we consider the initial function $\phi(x) = A\left(\frac{1}{4} - x\right)\left(\frac{1}{2} - x\right)\left(\frac{3}{4} - x\right)$ for various values of A.

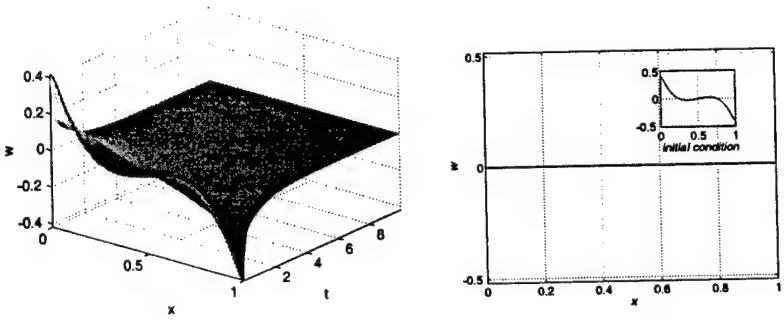

FIG. 6. Initial data $\phi(x) = 5\left(\frac{1}{4} - x\right)\left(\frac{1}{2} - x\right)\left(\frac{3}{4} - x\right)$ and final time $T = 10$

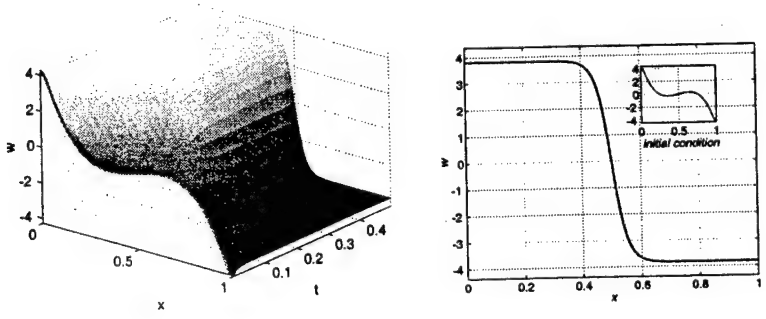

FIG. 7. Initial data $\phi(x) = 50\left(\frac{1}{4} - x\right)\left(\frac{1}{2} - x\right)\left(\frac{3}{4} - x\right)$ and final time $T = 0.25$

Once again we see that for A small, as $t \to \infty$ the numerical solution converges to zero, as it should. But for a larger amplitude A the numerical solution converges to a nonconstant steady state.

Finally we take the *negative* of the initial data that gave rise to numerical solutions which converged to nonconstant steady states and we note that these solutions tend to zero very quickly. Consequently, nonconstant numerical steady state solutions do not occur simply because of larger magnitude initial data.

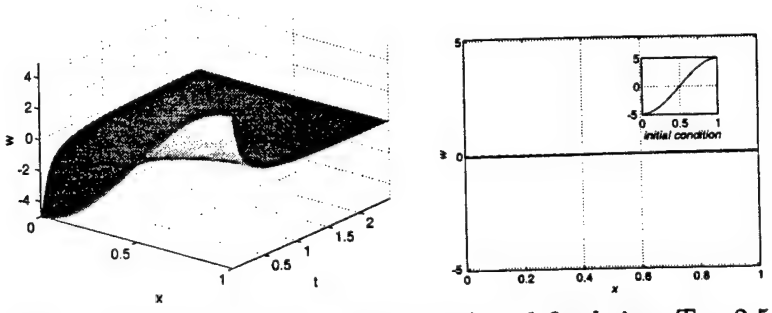

FIG. 8. Initial data $\phi(x) = -5\cos(\pi x)$ and final time $T = 2.5$

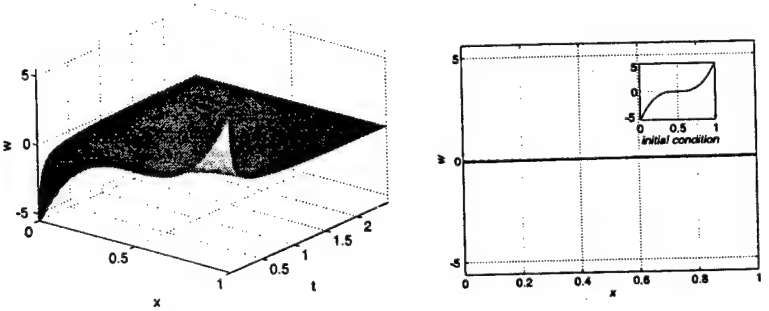

FIG. 9. Initial data $\phi(x) = -50(1/2 - x)^3$ and final time $T = 2.5$

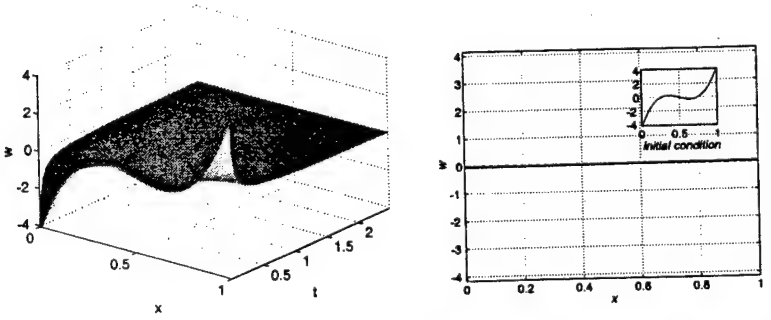

FIG. 10. Initial data $\phi(x) = -50\left(\frac{1}{4} - x\right)\left(\frac{1}{2} - x\right)\left(\frac{3}{4} - x\right)$
and
final time $T = 2.5$

initial data	T	c_0	$\|h-\widehat{h}\|_\infty$	$h'(0)$
$\cos(\pi(1/2-x))$	10.00	5.85e-06	8.57e-04	-5.85e-05
$5\cos(\pi(1/2-x))$	0.50	1.24e+01	8.08e-02	-7.65e-09
$-5\cos(\pi(1/2-x))$	2.50	8.71e-04	5.32e-02	-8.62e-03
$5(1/2-x)^3$	10.00	1.74e-07	2.74e-05	-1.74e-06
$50(1/2-x)^3$	0.50	1.56e+01	1.15e-01	-4.64e-10
$-50(1/2-x)^3$	2.50	5.44e-04	4.29e-02	-5.41e-03
$5\left(\frac{1}{4}-x\right)\left(\frac{1}{2}-x\right)\left(\frac{3}{4}-x\right)$	10.00	7.54e-08	1.18e-05	-7.54e-07
$50\left(\frac{1}{4}-x\right)\left(\frac{1}{2}-x\right)\left(\frac{3}{4}-x\right)$	0.50	7.31e+00	3.56e-02	-1.46e-06
$-50\left(\frac{1}{4}-x\right)\left(\frac{1}{2}-x\right)\left(\frac{3}{4}-x\right)$	2.50	2.84e-04	3.26e-02	-2.83e-03

TABLE I: Initial conditions, final time T, numerically computed c_0, maximum difference between $h(\cdot)$ and $\widehat{h}_j \equiv \widehat{h}(j\Delta x)$ for $j = 0, 1, \cdots, (N+1)$.

In order to draw attention to the actual functional values of the apparent nonconstant steady state, in the above examples we denote by $\widehat{h}(x)$ the numerically computed stationary solution. To be precise,

$$\widehat{h}(x) = \lim_{t\to\infty} w^{\Delta x}(x,t),$$

where $w^{\Delta x}(x,t)$ is computed by the Crank-Nicolson scheme described in the next section. We now let

$$c_0 = -\epsilon\widehat{h}_x(0) + \frac{\widehat{h}^2(0)}{2}.$$

In every Figure 2 - 10 the curves (plotted on the right side) depicting the numerical solution at the final time value T actually contain plots of both the numerical solution $\widehat{h}(\cdot)$ and the explicit function defined by equation (5.27) which only "nearly" satisfies the boundary conditions,i.e., $h'(0) = h'(1) = -\alpha$. Observe that $\widehat{h}(\cdot)$ and $h(\cdot)$ are not distinguishable on this scale. In Table I we have compiled a list for comparison of various parameters for our numerical examples. For all examples we have set $\epsilon = .1$ and $N = 80$ (the number of nodes for the Crank-Nicolson scheme).

5.2.4 A Symmetrized Crank-Nicolson Method

It has been observed that applying standard numerical methods to the system (5.19) for certain initial data in $L^2_{\mathrm{AS}}(0,1)$ produces numerical nonconstant steady state solutions.

However, Lemma 5.3 implies that not only must these solutions be constant, the constant must be zero. The objective of this section is to prove that the observed difficulty is due to the use of finite precision arithmetic. To do this we need to first obtain a very stable numerical scheme on which to base our proofs. The reason for this concern is that if, for example we employ a straightforward finite difference scheme to approximate (5.19) on the whole interval $(0,1)$, then no matter how small the spatial discretization or the time step size, eventually round-off error will corrupt the data at $x = 1/2$ (where the solution is known to be zero for all time). Because of this, there will always be a time at which the numerical method will undergo a rapid change and then generally converge to a nonzero constant. The sign of this constant depends on whether the value of the numerical solution first begins to drift positive or negative at $x = 1/2$. So our first step in obtaining a more stable numerical scheme consists of the reduction to a problem with a Dirichlet boundary condition at $x = 1/2$.

From Lemma 5.3 we see that for initial data $\phi \in L^2_{\rm AS}(0,1)$ we can replace problem (5.19) by the system

$$\begin{aligned} & w_t - \epsilon w_{xx} + w w_x = 0, \\ & x \in (0,1/2), \quad t > 0, \\ & w_x(0,t) = 0, \quad w(1/2,t) = 0, \\ & w(x,0) = \varphi(x). \end{aligned} \tag{5.32}$$

Thus, we need only solve the Burgers' equation on an interval of half the length and, more importantly for numerical calculations, we have replaced a Neumann boundary condition at $x = 1$ by a Dirichlet Boundary condition at $x = 1/2$.

Consider a standard implicit finite difference scheme for the system (5.32) on the interval $(0,1/2)$ with

$$x_i = i\Delta x, \ i = 0,1,2,\ldots,N, \ \ \Delta x = \frac{1}{(2N)},$$

$$\widetilde{\gamma} = \frac{\Delta t}{2\Delta x}, \ \ \kappa = \epsilon \frac{\Delta t}{(\Delta x)^2}, \ t_j = j\Delta t, \ \ j = 0,1,2,\ldots,$$

and, in a standard notation, define the approximation

$$w_{i,j} \approx w(x_i, t_j), \quad i = 0,1,2,\ldots,N, \ \ j = 0,1,2,\ldots.$$

Then, we have for $i = 1,2,\cdots,(N-2)$

$$\begin{aligned} w_{i,j+1} =& w_{i,j} + \frac{\kappa}{2}\left[w_{i+1,j} - 2w_{i,j} + w_{i-1,j}\right] \\ & + \frac{\kappa}{2}\left[w_{i+1,j+1} - 2w_{i,j+1} + w_{i-1,j+1}\right] \\ & + \frac{\widetilde{\gamma}}{2} w_{i,j}\left[w_{i+1,j} - w_{i-1,j}\right] + \frac{\widetilde{\gamma}}{2} w_{i,j+1}\left[w_{i+1,j} - w_{i-1,j}\right], \end{aligned} \tag{5.33}$$

and for $i = 0$ and $i = N-1$ we have

$$w_{0,j+1} = w_{0,j} + \frac{\kappa}{2}\left[2w_{1,j} - 2w_{0,j}\right] + \frac{\kappa}{2}\left[2w_{1,j+1} - 2w_{0,j+1}\right], \tag{5.34}$$

$$\begin{aligned} w_{N-1,j+1} =& w_{N-1,j} + \frac{\kappa}{2}\left[-2w_{N-1,j} + w_{N-2,j}\right] \\ &+ \frac{\kappa}{2}\left[-2w_{N-1,j+1} + w_{N-2,j+1}\right] \\ &+ \frac{\widetilde{\gamma}}{2} w_{N-1,j} w_{N-2,j} + \frac{\widetilde{\gamma}}{2} w_{N-1,j+1} w_{N-2,j+1}. \end{aligned} \tag{5.35}$$

Note that to obtain (5.34), we let

$$(w_{1,j} - w_{-1,j})/(2\Delta x) = 0 \quad \text{and} \quad w_{N,j} = 0 \quad \text{for all} \quad j \geq 0.$$

For this difference scheme let

$$\mathbf{w}_j = \begin{bmatrix} w_{-N+1,j} \\ w_{-N+2,j} \\ \vdots \\ w_{N-2,j} \\ w_{N-1,j} \end{bmatrix}$$

denote the solution at time step t_j. Then, we shall prove the following result.

Theorem 5.4 *For any piecewise continuous initial data $w(x,0) \in L^2_{AS}(0,1)$ and N sufficiently large*

$$\|\mathbf{w}_j\|_2 \xrightarrow{j\to\infty} 0.$$

That is, for every initial condition in $L^2_{\mathrm{AS}}(0,1)$, the finite difference solution converges, for every N sufficiently large, and the resulting limit is zero.

For analysis purposes, it is useful to extend this difference scheme to the symmetric interval $(-1/2, 1/2)$ with Dirichlet conditions at each end as long as we note that in the approximations of the first derivative terms the signs must be reversed. Thus, for $i = -N+2, -N+3, \ldots, -1$ we have

$$\begin{aligned} w_{i,j+1} =& w_{i,j} + \frac{\kappa}{2}\left[w_{i+1,j} - 2w_{i,j} + w_{i-1,j}\right] \\ &+ \frac{\kappa}{2}\left[w_{i+1,j+1} - 2w_{i,j+1} + w_{i-1,j+1}\right] \\ &- \frac{\widetilde{\gamma}}{2} w_{i,j}\left[w_{i+1,j} - w_{i-1,j}\right] - \frac{\widetilde{\gamma}}{2} w_{i,j+1}\left[w_{i+1,j} - w_{i-1,j}\right], \end{aligned} \tag{5.36}$$

with

$$\begin{aligned} w_{-N+1,j+1} =& w_{-N+1,j} + \frac{\kappa}{2}\left[-2w_{-N+1,j} + w_{-N+2,j}\right] \\ &+ \frac{\kappa}{2}\left[-2w_{-N+1,j+1} + w_{-N+2,j+1}\right] \\ &- \frac{\widetilde{\gamma}}{2} w_{-N+1,j} w_{-N+2,j} - \frac{\widetilde{\gamma}}{2} w_{-N+1,j+1} w_{-N+2,j+1}. \end{aligned} \tag{5.37}$$

The resulting difference scheme can be written in vector form as

$$\widetilde{A}\mathbf{w}_{j+1} = \widetilde{B}\mathbf{w}_j + \frac{\widetilde{\gamma}}{2}\mathbf{W}_j + \frac{\widetilde{\gamma}}{2}\mathbf{W}_{j+1}, \tag{5.38}$$

where

$$\widetilde{A} = \begin{bmatrix} 1+\kappa & -\frac{\kappa}{2} & & 0 \\ -\frac{\kappa}{2} & 1+\kappa & -\frac{\kappa}{2} & \\ & \ddots & & \\ 0 & & -\frac{\kappa}{2} & 1+\kappa \end{bmatrix}, \quad \widetilde{B} = \begin{bmatrix} 1-\kappa & \frac{\kappa}{2} & & 0 \\ \frac{\kappa}{2} & 1-\kappa & \frac{\kappa}{2} & \\ & \ddots & & \\ 0 & & \frac{\kappa}{2} & 1-\kappa \end{bmatrix},$$

$$\mathbf{W}_j = \begin{bmatrix} w_{-N+1,j}w_{-N+2,j} \\ w_{-N+2,j}\left(w_{-N+1,j} - w_{-N+3,j}\right) \\ \vdots \\ w_{N-2,j}\left(w_{N-3,j} - w_{N-1,j}\right) \\ w_{N-1,j}w_{N-2,j} \end{bmatrix},$$

$$\mathbf{W}_{j+1} = \begin{bmatrix} w_{-N+1,j+1}w_{-N+2,j+1} \\ w_{-N+2,j+1}\left(w_{-N+1,j+1} - w_{-N+3,j+1}\right) \\ \vdots \\ w_{N-2,j+1}\left(w_{N-3,j+1} - w_{N-1,j+1}\right) \\ w_{N-1,j+1}w_{N-2,j+1} \end{bmatrix}.$$

After simplification this system can be written as

$$A\mathbf{w}_{j+1} = -B\mathbf{w}_j - \frac{\widetilde{\gamma}}{\kappa}\mathbf{W}_j - \frac{\widetilde{\gamma}}{\kappa}\mathbf{W}_{j+1}, \tag{5.39}$$

with

$$A = \begin{bmatrix} -2-\frac{2}{\kappa} & 1 & & 0 \\ 1 & -2-\frac{2}{\kappa} & 1 & \\ & \ddots & & \\ 0 & & 1 & -2-\frac{2}{\kappa} \end{bmatrix}, \quad B = \begin{bmatrix} \frac{2}{\kappa}-2 & 1 & & 0 \\ 1 & \frac{2}{\kappa}-2 & 1 & \\ & \ddots & & \\ 0 & & 1 & \frac{2}{\kappa}-2 \end{bmatrix}. \tag{5.40}$$

It is well known that the matrix A is invertible and so once again we can rewrite the system (5.40) as

$$\mathbf{w}_{j+1} = -A^{-1}B\mathbf{w}_j - \frac{\widetilde{\gamma}}{\kappa}A^{-1}\mathbf{W}_j - \frac{\widetilde{\gamma}}{\kappa}A^{-1}\mathbf{W}_{j+1}, \tag{5.41}$$

and thus we have

$$\|\mathbf{w}_{j+1}\|_2 \leq \|A^{-1}B\|_2\|\mathbf{w}_j\|_2 + \frac{\widetilde{\gamma}}{\kappa}\|A^{-1}\|_2\|\mathbf{W}_j\|_2 + \frac{\widetilde{\gamma}}{\kappa}\|A^{-1}\|_2\|\mathbf{W}_{j+1}\|_2. \tag{5.42}$$

We need the following result in order to prove Theorem 5.4.

Lemma 5.5 *The eigenvalues of the* $(m-1)\times(m-1)$ *tri-diagonal matrix*

$$T = \begin{bmatrix} \alpha & 1 & & 0 \\ 1 & \alpha & 1 & \\ & & \ddots & \\ 0 & & 1 & \alpha \end{bmatrix}$$

are

$$(2+\alpha) - 4\sin^2\left(\frac{i\pi}{2m}\right), \quad i = 1, 2, \ldots, 2m-1. \tag{5.43}$$

Thus, the eigenvalues of A *are*

$$-\frac{2}{\kappa} - 4\sin^2\left(\frac{i\pi}{2N}\right), \quad i = 1, 2, \ldots, 2N-1,$$

and the eigenvalues of $A^{-1}B$ *are*

$$\beta_i \equiv \frac{\dfrac{2}{\kappa} - 4\sin^2\left(\dfrac{i\pi}{4N}\right)}{-\dfrac{2}{\kappa} - 4\sin^2\left(\dfrac{i\pi}{4N}\right)}, \quad i = 1, 2, \ldots, 2N-1. \tag{5.44}$$

Proof. (of Theorem 5.4) Let

$$\|A^{-1}B\|_2 = \beta = \max_{1\le i\le 2N-1} \beta_i, \quad \text{and notice that } \beta < 1.$$

Since

$$\|A^{-1}\|_2 \le \frac{\kappa}{2},$$

we have

$$\|\mathbf{w}_{j+1}\|_2 = \beta\|\mathbf{w}_j\|_2 + \frac{\widetilde{\gamma}}{2}\|\mathbf{W}_j\|_2 + \frac{\widetilde{\gamma}}{2}\|\mathbf{W}_{j+1}\|_2,$$

and the inequalities

$$\|\mathbf{W}_j\|_2 \le 2\|\mathbf{w}_j\|_2^2, \quad \|\mathbf{W}_{j+1}\|_2 \le 2\|\mathbf{w}_{j+1}\|_2^2,$$

imply

$$\|\mathbf{w}_{j+1}\|_2 \le \beta\|\mathbf{w}_j\|_2 + \widetilde{\gamma}\|\mathbf{w}_j\|_2^2 + \widetilde{\gamma}\|\mathbf{w}_{j+1}\|_2^2. \tag{5.45}$$

If $\zeta = \|\mathbf{w}_{j+1}\|_2$, $s = \|\mathbf{w}_j\|_2$, then (5.45) can be written as

$$\zeta \le \beta s + \widetilde{\gamma}s^2 + \widetilde{\gamma}\zeta^2.$$

Define $r = \beta s + \widetilde{\gamma}s^2$ and so $\widetilde{\gamma}\zeta^2 - \zeta + r \ge 0$ so that ζ must satisfy

$$\zeta \le \frac{1-\sqrt{1-4\widetilde{\gamma}r}}{2\widetilde{\gamma}} \le \frac{(4\widetilde{\gamma}r/2) + (2/9)(4\widetilde{\gamma}r)^2}{2\widetilde{\gamma}}, \quad \text{for } 4\widetilde{\gamma}r \le 3/4. \tag{5.46}$$

In order to justify the last inequality, we show that for $0 \leq \xi \leq 3/4$

$$1 - \sqrt{1-\xi} \leq \frac{\xi}{2} + \frac{2\xi^2}{9}.$$

This inequality follows from the chain of implications

$$0 \leq \xi \leq \frac{3}{4}$$
$$\left(\frac{1}{2} + \frac{2\xi}{9}\right)^2 \leq \left(\frac{2}{3}\right)^2$$

Rearranging and multiplying by ξ^2, gives

$$-\frac{4}{9}\xi^2 + \left(\frac{\xi}{2} + \frac{2}{9}\xi^2\right)^2 \leq 0.$$

Adding $(1-\xi)$ to both sides and rearranging terms gives

$$1 - 2\left(\frac{\xi}{2} + \frac{2\xi^2}{9}\right) + \left(\frac{\xi}{2} + \frac{2\xi^2}{9}\right)^2 \leq 1 - \xi.$$

The left side of this expression is a perfect square so we have

$$1 - \frac{\xi}{2} - \frac{4}{9}\xi^2 \leq \sqrt{1-\xi},$$

and finally we have

$$1 - \sqrt{1-\xi} \leq \frac{\xi}{2} + \frac{2\xi^2}{9}.$$

Setting $\zeta = 4\widetilde{\gamma}r$ yields inequality (5.46).

Returning to the estimate (5.46) we have that if $4\widetilde{\gamma}r < 3/4$, then

$$\zeta \leq r + \frac{16\widetilde{\gamma}}{9}r^2.$$

Now choose ∂ so that $(\beta + \partial) < 1$. Suppose that, as a very conservative estimate, $s = \|\mathbf{w}_j\|_2 \leq \partial/(4\widetilde{\gamma})$. Then

$$r = \beta s + \widetilde{\gamma}s^2 \leq \left(\beta + \frac{\partial}{4}\right)s$$

and

$$\begin{aligned}\zeta &\leq \left(\beta + \frac{\partial}{4}\right)s + \frac{16\widetilde{\gamma}}{9}\left(\beta + \frac{\partial}{4}\right)s\frac{\partial}{4\widetilde{\gamma}} \\ &= \left(\beta + \frac{\partial}{4}\right)s + \frac{4}{9}\partial\left(\beta + \frac{\partial}{4}\right)s \\ &\leq (\beta + \partial)\, s.\end{aligned}$$

Hence, if $\|\mathbf{w}_j\|_2 \leq \partial/(4\widetilde{\gamma})$ then

$$\|\mathbf{w}_{j+1}\|_2 \leq (\beta + \partial)\|\mathbf{w}_j\|_2, \quad \text{where} \quad \beta + \partial < 1.$$

This implies that $\|\mathbf{w}_j\|_2 \to 0$ as $j \to \infty$, provided that $\|\mathbf{w}_0\|_2 \leq \partial/(4\widetilde{\gamma})$. Note also that when $\|\mathbf{w}_j\|_2 \leq \partial/(4\widetilde{\gamma})$, then $4\widetilde{\gamma}r \leq \partial\,(\beta + \partial/4) < \partial$. Thus, we also need $\partial < 3/4$.

Recalling the definition for $\widetilde{\gamma} = \Delta t/(2\Delta x)$ we have

$$\|\mathbf{w}_0\|_2 \leq \frac{\partial}{4\widetilde{\gamma}} \leq \frac{(1-\beta)\Delta x}{2\Delta t}$$

Generally we would require that Δt is somewhat smaller than Δx. Indeed, it is possible to take

$$\Delta t = \frac{\epsilon(\Delta x)^2}{4} < \frac{\epsilon(\Delta x)^2}{2}$$

so that the initial requirement would be

$$\|\mathbf{w}_0\|_2 \leq \frac{2(1-\beta)}{\epsilon\Delta x} = \frac{4(1-\beta)N}{\epsilon},$$

where in the last equality we have used $\Delta x = \dfrac{1}{2N}$. Therefore, we see that this condition is not really a restriction, except for numerical difficulties, since we can take N sufficiently large to include any given piecewise continuous initial data and this completes the proof. □

5.2.5 Stationary Solutions of Explicit Finite Difference Schemes

In this section we consider several explicit finite difference schemes for the problem (5.19) and make some observations concerning the existence of nonconstant stationary solutions for these discrete schemes. In this section we assume that N, the number of spatial nodes, is even and we set $\Delta x = 1/N$, for $i = 0, 1, \ldots$, $x_i = i\Delta x$ and $t_j = j\Delta t$. We consider three different schemes based on forward difference in time, central difference for the second order term, and three different approximations for the convective term. (Recall the notation $w_{ij} \approx w(x_i, t_j)$.)

Example 2 *Centered Difference ww_x:* For $i = 0, 1, 2, \cdots, N$

$$\frac{(w_{i,j+1} - w_{i,j})}{\Delta t} = \epsilon\left[\frac{w_{i+1,j} - 2w_{i,j} + w_{i-1,j}}{(\Delta x)^2}\right] - w_{i,j}\left[\frac{w_{i+1,j} - w_{i-1,j}}{(2\Delta x)}\right]. \tag{5.47}$$

$$w_{-1,j} = w_{1,j} \quad w_{N+1,j} = w_{N-1,j}.$$

The steady form of (5.47) is given in terms of a function $v(x)$ with $v_i = v(x_i)$ by

$$v_{i+1} - 2v_i + v_{i-1} - r_1 v_i\,(v_{i+1} - v_{i-1}) = 0, \quad i = 0, \ldots, N \tag{5.48}$$

$$v_{-1} = v_1, \quad v_{N+1} = v_{N-1} \quad \text{and} \quad r_1 = \frac{\Delta x}{2\epsilon}. \tag{5.49}$$

For this case (5.48) has one stationary solution, the constant solution, i.e., for any $c \in \mathbb{R}$, $v_i = c$ for $i = 0, 1, \ldots, N$ is a solution. But, there is another solution given by

$$v_i = \begin{cases} 0, & i = N/2 \\ 1/r_1, & 0 \leq i \leq N/2 - 1 \\ -1/r_1, & N/2 + 1 \leq i \leq N. \end{cases} \tag{5.50}$$

Example 3 *Centered Difference* $(w^2)_x/2$*:* For $i = 0, 1, 2, \cdots, N$

$$\frac{(w_{i,j+1} - w_{i,j})}{\Delta t} = \epsilon \left[\frac{w_{i+1,j} - 2w_{i,j} + w_{i-1,j}}{(\Delta x)^2} \right] - \frac{1}{2} \left[\frac{w_{i+1,j}^2 - w_{i-1,j}^2}{(2\Delta x)} \right] \tag{5.51}$$

$$w_{-1,j} = w_{1,j} \quad w_{N+1,j} = w_{N-1,j}.$$

The steady form of (5.51) is

$$v_{i+1} - 2v_i + v_{i-1} - r_2 \left(v_{i+1}^2 - v_{i-1}^2 \right) = 0, \quad i = 0, \ldots, N \tag{5.52}$$

$$v_{-1} = v_1, \quad v_{N+1} = v_{N-1} \quad \text{and} \quad r_2 = \frac{\Delta x}{4\epsilon}. \tag{5.53}$$

For this case (5.52) has a solution $v_i = c$ for $i = 0, 1, \ldots, N$ for any $c \in \mathbb{R}$. Again there is a second solution given by

$$v_i = \begin{cases} 0, & i = N/2 \\ 1/r_2, & 0 \le i \le N/2 - 1 \\ -1/r_2, & N/2 + 1 \le i \le N. \end{cases} \tag{5.54}$$

Example 4 *Forward Difference* ww_x*:* For $i = 1, 2, , N - 1$

$$\frac{(w_{i,j+1} - w_{i,j})}{\Delta t} = \epsilon \left[\frac{w_{i+1,j} - 2w_{i,j} + w_{i-1,j}}{(\Delta x)^2} \right] - w_{i,j} \left[\frac{w_{i,j} - w_{i-1,j}}{(\Delta x)} \right] \tag{5.55}$$

$$w_{0,j} = w_{1,j} \quad w_{N,j} = w_{N-1,j}.$$

The steady form of (5.55) is

$$v_{i+1} - 2v_i + v_{i-1} - r_3 v_i \left(v_i - v_{i-1} \right) = 0, \quad i = 1, \ldots, N - 1 \tag{5.56}$$

$$v_0 = v_1, \quad v_N = v_{N-1} \quad \text{and} \quad r_3 = \frac{\Delta x}{\epsilon}. \tag{5.57}$$

However, in this case, one can show that the only stationary solution is the constant solution $v_i = c$ for $i = 1, \ldots, N - 1$.

The above examples illustrate that discrete versions of the steady state problems can have non-constant discrete solutions. Thus, if one uses one of the methods (5.47) or (5.51), then any numerical algorithm (time marching, direct, etc.) could produce a discrete non-constant stationary solution. This can happen even when the original partial differential equation does not have such nonconstant stationary solutions. Thus, the numerical stationary solutions are not approximate solutions to the steady state partial differential equation (plus boundary conditions).

On the other hand, the scheme (5.56) only has constant discrete stationary solutions. Therefore, one might expect that if the discrete equations (5.56) are used then numerical solutions based on this type of algorithm will not produce false solutions. However, because of finite precision arithmetic, this assumption is not valid.

5.2.6 The Effect of Finite Precision Arithmetic

In reality, all calculations are done in finite precision arithmetic. Even calculations using computer algebra systems that purport to be capable of infinite precision are actually limited by memory and storage limitations. More realistically, floating point arithmetic is commonly used in computational work and floating point arithmetic is based on a finite set of numbers and a finite precision arithmetic. Furthermore different machines have a different set of numbers and precision. We plan to show, by way of examples, that the reason for the anomaly observed in this work is due to the necessary use of finite precision arithmetic. We have already seen in the last section that using exact arithmetic the symmetrized Crank-Nicolson numerical scheme must converge to zero for initial data in $L^2_{\rm AS}(0,1)$. In this section we show that by altering only the magnitude of the initial data, the value of the viscosity ϵ and the precision, we can generate solutions that converge either to zero or to one of the analytic solutions that only approximately satisfy the boundary conditions. We note that for ϵ fairly large (for example $\epsilon = 1/2$) convergence to a nonconstant numerical stationary solution requires larger magnitude initial data and for smaller ϵ we can take the magnitude to be much smaller. (Note that the Crank-Nicolson scheme is used for all the calculations in this section.)

In our first example we consider an initial condition which happens also to correspond to a possible fixed point of the finite centered difference scheme used in Example 2. Fix N, ϵ, and $U > 0$, then define the initial data

$$\phi(x) = \begin{cases} U, & 0 \le x < 1/2 \\ 0, & x = 1/2 \\ -U, & 1/2 < x \le 1 \end{cases} . \tag{5.58}$$

Although we do not include the proof here, we have shown that, with full (infinite) precision arithmetic, the spatially centered difference spatial discretization and Euler marching scheme for $U < 1/r_1 = 2N\epsilon$ converges to zero with increasing time. Thus, this example provides a good test for our hypotheses that numerical stationary solutions arise from finite precision arithmetic.

In this numerical example, we take $N = 40$ and $\epsilon = 1/5$ so that in (5.50) $r_1 = 1/16$. Thus, a stationary solution for the centered difference method is given by

$$v(x) = \begin{cases} 1/r_1, & 0 \le x < 1/2 \\ 0, & x = 1/2 \\ -1/r_1, & 1/2 < x \le 1 \end{cases} . \tag{5.59}$$

For the first numerical run we take initial data with $U = 8$ and we successively choose the number of significant digits to be $d = 4, 8, 16$ for numerical simulation.

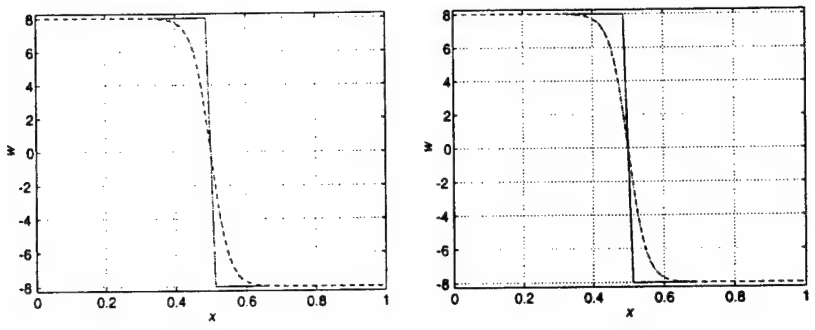

$d = 4$ $d = 8$

d=16

FIG. 11. Piecewise Constant Initial Condition $U = 8$

Notice, as shown in the following table, that the values continue to drop for $d = 16$ while a steady state is reached for $d = 4$ and $d = 8$.

t	d $= 4$	d $= 8$	d $= 16$
0	8.00000000000000	8.00000000000000	8.00000000000000
10	7.99900000000000	8.00000000000000	7.99985129822842
20	7.99900000000000	8.00000000000000	7.99970174625331
30	7.99900000000000	8.00000000000000	7.99955214983113
40	7.99900000000000	8.00000000000000	7.99940250894646
50	7.99900000000000	8.00000000000000	7.99925282355433
60	7.99900000000000	8.00000000000000	7.99910309364852
70	7.99900000000000	8.00000000000000	7.99895331919820
80	7.99900000000000	8.00000000000000	7.99880350016796
90	7.99900000000000	8.00000000000000	7.99865363654645
100	7.99900000000000	8.00000000000000	7.99850372828631

TABLE II: Values at $x = 0$

Now consider a smaller value $U = 4$ and repeat the same calculations.

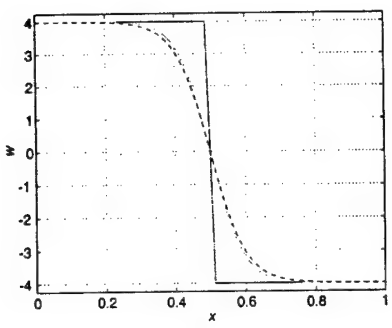

$d = 4$

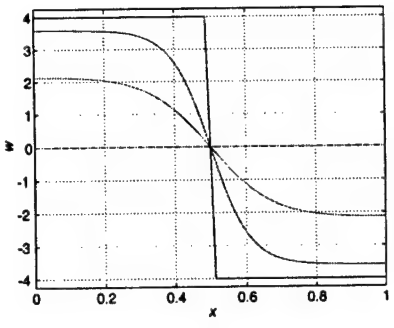

$d = 8$

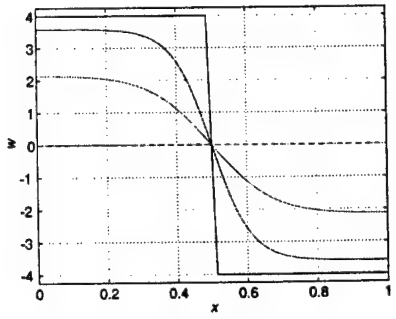

$d = 16$

FIG. 12. Piecewise Constant Initial Condition $U = 4$

Notice as shown in the Figure 11 and the following table, the computed values continue to decrease to zero for $d = 8$ and $d = 16$, but a non-constant solution is reached for $d = 4$.

t	d $= 4$	d $= 8$	d $= 16$
0	4.00000000000000	4.00000000000000	4.00000000000000
10	4.00000000000000	3.58872030000000	3.58892931217814
20	4.00000000000000	2.13481320000000	2.13685522204510
30	4.00000000000000	0.00000025606987	0.00000025848659
40	4.00000000000000	0.00000000000000	0.00000000000000
50	4.00000000000000	0.00000000000000	0.00000000000000
60	4.00000000000000	0.00000000000000	0.00000000000000
70	4.00000000000000	0.00000000000000	0.00000000000000
80	4.00000000000000	0.00000000000000	0.00000000000000
90	4.00000000000000	0.00000000000000	0.00000000000000
100	4.00000000000000	0.00000000000000	0.00000000000000

TABLE III: Values at $x = 0$

If we now take $U = 1/r = 16$ then the initial condition is a stationary solution for the particular values $N = 40$ and $\epsilon = 1/5$. Indeed, when we run the same calculation as above we obtain the plot given in Figure 13.

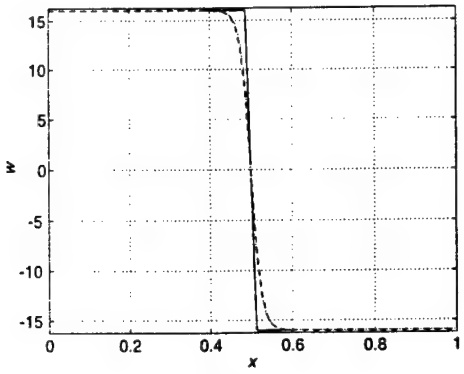

d=32

FIG. 13. Relation to Stationary Solution of Discrete Problem

In each case above, at each time step, we have also computed the numerical value of the derivative of the solution $\widetilde{w}$ at $x = 0$ and used the fact that

$$c_0 = \frac{w(0,t)^2}{2} - \epsilon \frac{w_x(0,t)}{2}$$

to obtain

$$c_0^j = \frac{\widetilde{w}_{0,j}^2}{2} - \epsilon \left(\frac{w_{1,j} - w_{0,j}}{\Delta x} \right).$$

At each time step the above graphs also include the graph of

$$h_j(x) = \sqrt{2c_0^j} \tanh \left(\frac{\sqrt{2c_0^j}}{4\epsilon} \right)$$

whose derivative at zero is

$$w_x(0,t_j) \approx w_{jx}(0) = -\frac{c_0^j}{\epsilon} \operatorname{sech} \left(\frac{\sqrt{2c_0^j}}{4\epsilon} \right)^2.$$

In the last case we have $c_0^j = 128.0$ for all j and the approximation to the derivative is

$$w_{jx}(0) = -1.09\,10^{-14}$$

5.2.7 Finite Arithmetic and Convergence to Steady State

Let β denote the base for a computer system and t the number of digits. On the interval $[\beta^{m-1}, \beta^m]$, the floating point numbers are evenly spaced with separation β^{m-t}.

FIG. 14. Floating Point Numbers $\alpha_2 = \alpha_1 + \beta^{m-t}$

Let $x_1, x_2 \in [\beta^{m-1}, \beta^m]$ be two floating point numbers. If $|x_1 - x_2| < \frac{1}{2}\beta^{m-t}$, then $x_1 = x_2$. Thus, if

$$|x_1 - x_2| < \frac{1}{2}\beta^{1-t}\beta^{m-1} \leq \frac{1}{2}\beta^{1-t}|x_1|,$$

or, if

$$\frac{|x_1 - x_2|}{|x_1|} < \frac{1}{2}\beta^{1-t},$$

then $x_1 = x_2$.

Consider the non-homogeneous problem for Burgers' equation on the interval $[0, 1/2]$ given by

$$\begin{aligned} &w_t - \epsilon w_{xx} + w w_x = 0, \\ &w_x(0,t) = -\alpha, \quad \alpha > 0, \\ &w(1/2,t) = 0 \\ &w(x,0) = \phi(x), \end{aligned} \tag{5.60}$$

If $\alpha = 0$ then we know from Theorem 5.2 that $w(x,t) \to 0$ as $t \to \infty$. If $\alpha \neq 0$ we expect from our numerical evidence (and the discussion in the next section) that

$$w(x,t) \xrightarrow{t\to\infty} h(x) = \sqrt{2c_0}\tanh\left(\frac{\sqrt{2c_0}}{2\epsilon}(1/2 - x)\right),$$

where

$$h'(0) - \frac{c_0}{\epsilon}\mathrm{sech}^2\left(\frac{\sqrt{2c_0}}{4\epsilon}\right) = -\alpha.$$

Consider the Crank-Nicolson scheme for (5.60) and let

$$\frac{(w_{1,j} - w_{-1,j})}{2\Delta x} = -\alpha,$$

so that

$$w_{1,j} = -2\alpha(\Delta x) + w_{-1,j}.$$

It follows that

$$w_{-1,j} = w_{1,j}\left[1 + \frac{2\alpha\Delta x}{w_{1,j}}\right] \approx w_{1,j}\left[1 + \frac{2\alpha\Delta x}{w_{0,j}}\right],$$

and hence, if $2\alpha(\Delta x)/w_{0,j} < (1/2)\beta^{1-t}$, then $w_{-1,j} = w_{1,j}$. This implies that the condition

$$\frac{(w_{1,j} - w_{-1,j})}{2\Delta x} = 0,$$

is equivalent to

$$\frac{(w_{1,j} - w_{-1,j})}{2\Delta x} = -\alpha,$$

if

$$\frac{2\alpha(\Delta x)}{w_{0,j}} < \frac{1}{2}\beta^{1-t}.$$

Thus, even when $\alpha = 0$ the solution on any computer may converge to (approximately) $h(x)$.

In order to examine this more closely, consider the inequality

$$\frac{2\alpha(\Delta x)}{w_{0,j}} < \frac{1}{2}\beta^{1-t}.$$

It is reasonable to expect that $w_{0,j} \approx \phi(0)$ if a nonzero steady state is quickly reached. Consequently, if

$$\frac{\sqrt{2c_0}}{4\epsilon} \gg 1,$$

then

$$\phi(0) \approx h(0) \approx \sqrt{2c_0}.$$

Assuming that $\dfrac{\sqrt{2c_0}}{4\epsilon} \gg 1$, we have

$$\alpha \approx 4\frac{c_0}{\epsilon} \exp\left(\frac{-\sqrt{2c_0}}{2\epsilon}\right),$$

and

$$\frac{2\alpha(\Delta x)}{w_{0,j}} < \frac{1}{2}\beta^{1-t}$$

can be approximated by

$$\frac{8(\Delta x)\phi(0)}{2\epsilon} \exp\left(\frac{-\phi(0)}{2\epsilon}\right) < \frac{1}{2}\beta^{1-t}. \tag{5.61}$$

Consider once again the numerical example above with initial data given by (5.58) restricted to the interval $[0, 1/2]$. In particular, we take

$$\phi(x) = \begin{cases} U, & 0 \le x < 1/2 \\ 0, & x = 1/2 \end{cases}. \tag{5.62}$$

We take $\phi(0) = U$, the number of digits $d = t$, $\beta = 10$, $\delta x = 1/80$, $\epsilon = 1/5$ and for the numerical scheme we have taken a time step size of $\delta t = 1/4000$. If

$$\frac{U}{4} \exp\left(\frac{-5U}{2}\right) < \frac{1}{2}10^{1-d},$$

we expect the computed solution may approach a nonzero steady state.

For $U = 4$ and $d = 5$ we have

$$\frac{U}{4} \exp\left(\frac{-5U}{2}\right) = 0.4539992976248510^{-4} < 0.5 \times 10^{-4} = \frac{1}{2}10^{1-d},$$

so we expect that the solution will converge to a nonzero steady state.

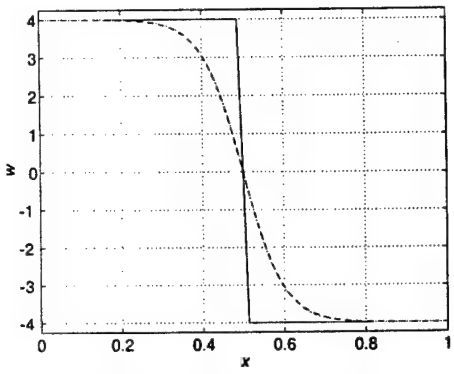

FIG. 15. Trajectories at $t_j = 10j$, $j = 0, 1, \cdots, 10$ with $d = 5$

For $U = 4$ and $d = 6$ we have

$$\frac{U}{4}\exp\left(\frac{-5U}{2}\right) = 0.4539992976248510^{-4} > 0.05 \times 10^{-4} = \frac{1}{2}10^{1-d}$$

so we expect that the solution will converge to a zero. This behavior is demonstrated in Figures 15, 16 and Table IV.

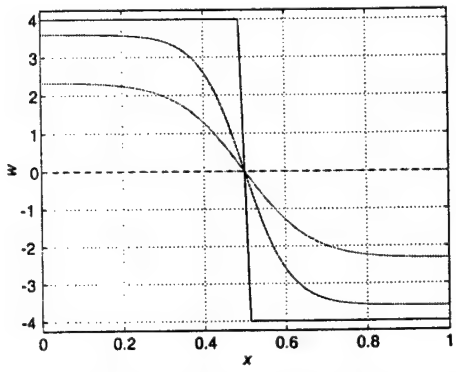

FIG. 16. Trajectories at $t_j = 10j$, $j = 0, 1, \cdots, 10$ with $d = 6$

t	d $= 5$	d $= 6$
10.00	4.000000	3.60426000000
20.00	4.00000	2.32885000000
30.00	4.00000	0.000000737544
40.00	4.00000	0.000000000000
50.00	4.00000	0.000000000000
60.00	4.00000	0.000000000000
70.00	4.00000	0.000000000000
80.00	4.00000	0.000000000000
90.00	4.00000	0.000000000000
100.00	4.0000	0.000000000000

TABLE IV

5.2.8 Sensitivity and Stability Analysis

For a small positive number α we replace the problem (5.19) in $L^2_{\mathrm{AS}}(0,1)$ with homogeneous Neumann boundary conditions by the following problem with non-homogeneous Neumann boundary conditions:

$$\begin{aligned} &w_t - \epsilon w_{xx} + w w_x = 0, \ x \in (0,1), \\ &x \in (0,1), \quad t > 0 \\ &w_x(0,t) = w_x(1,t) = -\alpha, \quad \alpha > 0, \\ &w(x,0) = \phi(x). \end{aligned} \tag{5.63}$$

We show below that solutions of (5.63) are highly sensitive to the boundary condition parameter α.

For $\phi \in L^2_{\mathrm{AS}}(0,1)$ the solution $w(\cdot,t)$ remains in $L^2_{\mathrm{AS}}(0,1)$ for all $t > 0$ by Theorem 5.3. Therefore, the Burgers' problem (5.63) is equivalent to

$$\begin{aligned} &w_t - \epsilon w_{xx} + w w_x = 0, \ x \in (0,1/2), \ t > 0 \\ &w_x(0,t) = -\alpha, \quad w(1/2,t) = 0, \quad \alpha > 0, \\ &w(x,0) = \phi(x). \end{aligned} \tag{5.64}$$

The stationary problem associated with (5.64) isgiven earlier in (5.30), (5.31). We also note that in $L^2_{\mathrm{AS}}(0,1)$ we can replace this problem by the equivalent problem

$$\epsilon v_{xx} - v v_x = 0, \quad x \in (0,1), \tag{5.65}$$

$$v_x(0) = -\alpha, \ v(1/2) = 0. \tag{5.66}$$

which, for numerical work, is more tenable.

As we have noted, the function (5.27) satisfies stationary Burgers' equation and the derivative at $x = 0, 1$ satisfies (5.31) (and (5.66)) provided

$$h'(0) = h'(1) = -\alpha. \tag{5.67}$$

This amounts to finding c_0 that satisfies the equation

$$\frac{c_0}{\epsilon} \operatorname{sech}^2\left(\frac{\sqrt{2c_0}}{4\epsilon}\right) = \alpha. \tag{5.68}$$

In the space $L^2_{\mathrm{AS}}(0,1)$ there are exactly two solutions of (5.68) for α small enough. Namely, there exist $c_0^< \approx 0$ and $c_0^> \gg 0$ giving

$$h^<(x) = \sqrt{2c_0^<} \tanh\left(\frac{\sqrt{2c_0^<}}{2\epsilon}(1/2 - x)\right) \tag{5.69}$$

$$h^>(x) = \sqrt{2c_0^>} \tanh\left(\frac{\sqrt{2c_0^>}}{2\epsilon}(1/2 - x)\right) \tag{5.70}$$

and these functions satisfy the nonhomogeneous boundary conditions

$$h_x(0) = -\alpha, \quad h_x(1) = -\alpha.$$

To see that there are exactly two such values of c_0 for small α, let $s = \sqrt{c_0}/(2\sqrt{2}\epsilon)$ so that equation (5.68) becomes

$$s^2\text{sech}^2(s) = \frac{\alpha}{8\epsilon}.$$

The function $f(s) = s^2\text{sech}^2(s)$ has a critical value at $s_0 \approx 1.2$. This allows us to conclude that the maximum value of f is $M_\epsilon = 8\epsilon s_0^2\text{sech}^2(s_0)$. From the graph of f in Figure 17, it is clear that this maximum imposes a smallness constraint on α. Namely, in order for the conditions in (5.67) to be satisfied, we need

$$\alpha \leq M_\epsilon.$$

For fixed ϵ and α sufficiently small, we see that there are two solutions given by (5.69) and (5.70) and both functions satisfy the conditions in (5.67).

The solution $h^<(\cdot)$ is very nearly the zero function, whereas the solution $h^>(\cdot)$ is not usually small.

FIG. 17. Graph of f, for $\epsilon = .01$ and $\alpha = .007$

FIG. 18. Graph of $h^<(\cdot)$, for $\epsilon = .01$ and $c_0 = 7.7287e - 05$

FIG. 19. Graph of $h^>(\cdot)$, for $\epsilon = .01$ and $c_0 = .0072$

In each of Figures 18 and 19 there is actually two functions plotted, $\widehat{h}$ computed numerically and also from the formula (5.27).

A complete analysis of the mathematical validity of these stationary solutions for Burgers' equation involves a careful analysis of the long time behavior of solutions to the dynamical system

$$\begin{aligned} &w_t - \epsilon w_{xx} + ww_x = f_\alpha \\ &w_x(0,t) = w_x(1,t) = 0, \\ &w(x,0) = \phi(x), \\ &f_\alpha = \alpha(\delta_0 - \delta_1) \in \widetilde{H}^{-1}(0,1) \end{aligned}$$

Here, δ_a denotes the δ-function concentrated at $x = a$. and by $\widetilde{H}^{-1}(0,1)$ we denote the dual of $H^1(0,1)$ which consists of all distributions from $H^{-1}(\mathbb{R})$ whose support belongs to

$[0,1]$. For small α and small initial conditions ϕ, one knows that global in time existence of solutions to the above system and the existence of a compact local attractor. Unfortunately, for larger initial conditions these results do not apply for f_α as above.

5.2.9 Linearization about Numerical Stationary Solution

To determine the stability properties of these stationary solutions we follow the development for a similar problem given by Kreiss. Namely, after a reduction to the interval $(0,1/2)$, we consider the spectral analysis of the linearization of the Burgers' system (5.63) in $L^2_{\rm AS}(0,1/2)$ about the function $h(\cdot)$ in (5.27). We will show that for a fixed ϵ, the first eigenvalue of this linear problem is negative if c_0 is small. But for larger c_0 this eigenvalue becomes positive and then decreases monotonically to zero. The remaining eigenvalues of the linearized problem are all negative. Thus for c_0 small the stationary solution is stable and for the larger value of c_0 the corresponding stationary solution is unstable. However, the first eigenvalue, which is positive, is so small that the dynamics still can converge to a nonconstant stationary value.

To this end, let

$$w = h + \delta z, \quad z \in L^2_{\rm AS}(0,1),$$

substitute this into (5.63) and collect terms of order one in δ to obtain

$$\begin{aligned} &z_t - \epsilon w_{xx} + (hz)_x = 0, \\ &x \in (0,1), \quad t > 0 \\ &z_x(0,t) = z_x(1,t) = 0, \quad \alpha > 0, \\ &z(x,0) = z_0(x), \end{aligned} \tag{5.71}$$

where generally we assume that z_0 is small in $L^2_{\rm AS}(0,1)$.

We can replace this problem with the numerically stable problem on the half interval $(0,1/2)$ given by

$$\begin{aligned} &z_t - \epsilon w_{xx} + (hz)_x = 0, \\ &x \in (0,1), \quad t > 0 \\ &z_x(0,t) = z(1/2,t) = 0, \quad \alpha > 0, \\ &z(x,0) = z_0(x). \end{aligned} \tag{5.72}$$

Associated with this problem we consider the spectral problem

$$\epsilon\varphi_{xx} - (h\varphi)_x = \lambda\varphi, \quad \varphi_x(0) = \varphi(1/2) = 0. \tag{5.73}$$

It is useful for computations to replace this eigenvalue problem by a self-adjoint problem, so we let

$$\eta = \exp\left(\int_{1/2}^{x} h(s)\,ds\right) = \operatorname{sech}\left(\frac{\sqrt{2c_0}}{2\epsilon}\left(\frac{1}{2} - x\right)\right), \tag{5.74}$$

and seek φ in the form

$$\varphi = \eta\psi.$$

After some straightforward calculations we find that the problem (5.73) can be replaced by the problem

$$\epsilon\psi_{xx} - q\psi = \lambda\psi, \quad \psi_x(0) = \psi(1/2) = 0. \tag{5.75}$$

where

$$q(x) = \frac{1}{4\epsilon}h^2 + \frac{1}{2}h_x.$$

Since h satisfies

$$-h_x + \frac{h^2}{2} = c_0$$

we have

$$q(x) = \left(\frac{c_0}{2\epsilon}\right)\left(1 - 2\text{sech}^2\left(\frac{\sqrt{2c_0}}{2\epsilon}(1/2 - x)\right)\right). \tag{5.76}$$

We must also consider the transformation of the boundary conditions. Note that

$$0 = \varphi_x(0) = \eta(0)\left(\psi_x(0) + \frac{1}{2\epsilon}h(0)\psi(0)\right),$$
$$0 = \varphi(1/2) = \eta(1/2)\psi(1/2) = \psi(1/2).$$

Thus, we arrive at the eigenvalue problem

$$L_\gamma\psi \equiv \psi_{xx} - q_\gamma\psi = \widetilde{\lambda}\psi, \tag{5.77}$$

subject to the boundary conditions

$$\psi_x(0) + \widetilde{\gamma}\psi(0) = 0, \quad \psi(1/2) = 0 \tag{5.78}$$

where

$$\widetilde{\gamma} = \frac{1}{2\epsilon}h(0), \quad \widetilde{\lambda} = \lambda/\epsilon, \quad g_\gamma = \gamma^2(1 - 2\text{sech}^2(\gamma(1/2 - x)). \tag{5.79}$$

As Kreiss noted the first eigenvalue of (5.77)-(5.78) satisfies

$$|\widetilde{\lambda}| \leq \frac{\|L_\gamma\psi\|}{\|\psi\|}$$

for all functions $\psi \in L^2(0, 1/2)$ that are sufficiently smooth and satisfy the boundary conditions (5.78).

Lemma 5.6 *If $\sqrt{2c_0}/(2\epsilon) > 4$, then there are positive constants C and D, independent of ϵ, so that the smallest eigenvalue of (5.77)-(5.78) satisfies*

$$\left|\widetilde{\lambda}_1\right| \leq \frac{C}{\epsilon}e^{-D\epsilon^{-1}}. \tag{5.80}$$

Let

$$\widetilde{\eta}(x) = \eta(x) - 2\eta(0)$$

where η is defined in (5.74). We note that $\widetilde{\eta}$ is a symmetric function about $x = 1/2$, it satisfies the boundary conditions (5.78) and is smooth. Also we have

$$L\widetilde{\eta} = 2q\eta(0).$$

Thus, we have the estimate

$$
\begin{aligned}
|\lambda_1|^2 &\le \frac{\|L\widetilde{\eta}\|^2}{\|\widetilde{\eta}\|^2} \\
&= \left(\int_0^{1/2} (2\eta(0)q(x))^2\,dx\right) \Big/ \left(\int_0^{1/2} (\eta(x)-2\eta(0))^2\,dx\right) \\
&= \left(\frac{4c_0^2}{\epsilon^2\cosh^2(\sqrt{2c_0}/(4\epsilon)}\right) \frac{\left(\int_0^{1/2} \left(1-2\mathrm{sech}^2(\sqrt{2c_0}/(2\epsilon)s)\right)^2\,ds\right)}{\left(\int_0^{1/2} \left(2\mathrm{sech}(\sqrt{2c_0}/(4\epsilon)) - \mathrm{sech}(\sqrt{2c_0}/(2\epsilon)s)\right)^2\,ds\right)} \\
&\le \frac{C^2}{\epsilon^2\exp\left(2D\epsilon\right)}.
\end{aligned}
$$

Here we have used the fact that $\mathrm{sech}(\sqrt{2c_0}/(2\epsilon)s))$ is a monotone decreasing function of s and the assumption $\gamma \equiv \sqrt{2c_0}/(2\epsilon) > 4$ which ensures that

$$
\left(\int_0^{1/2} (1-2\mathrm{sech}^2(\gamma s))^2\,ds\right) \le c_0 \left(\int_0^{1/2} (1-2\mathrm{sech}^2(\gamma/2)\mathrm{sech}(\gamma s))^2\,ds\right).
$$

Unlike the case of nonhomogeneous Dirichlet boundary conditions considered in by Kreiss, for nonhomogeneous Neumann conditions the resulting linearization about the equilibrium is not exponentially stable for all γ. In this case it is difficult to establish this analytically, so we only present the numerical results obtained for the first three eigenvalues computed for a range of values of γ (i.e., c_0 for fixed $\epsilon = .1$). For one value of c_0 we have plotted the corresponding normalized eigenfunctions. Note that when $c_0 = 0$ the problem (5.77), (5.78) reduces to

$$
\varphi'' = \widetilde{\lambda}\varphi, \quad \varphi'(0) = 0, \quad \varphi(1/2) = 0
$$

with eigenvalues given explicitly by $\lambda_j = -(2j-1)^2\pi^2$ for $j = 1, 2, \cdots$ and with associated eigenfunctions $\varphi_j(x) = \sqrt{2}\cos((2j-1)\pi x)$ for $j = 1, 2, \cdots$.

Thus, for small γ the problem has all stable eigenvalues. However, we show that as γ increases the first eigenvalue $\widetilde{\lambda}_1$, as a function of γ, becomes positive, stays positive and decreases to zero as γ tends to infinity.

We have fixed $\epsilon = .1$, set $\gamma = \dfrac{\sqrt{2c_0}}{2\epsilon}$ and varied c_0 from $c_0 = 0$ to $c_0 = 18$ so that γ varies from $\gamma = 0$ to $\gamma = 20$. The eigenfunctions are depicted in Figure 20 with $\gamma = 16$ (or $c_0 = 5.12$) while Figure 21 contains the plot of γ versus λ_j for $j = 1, 2$.

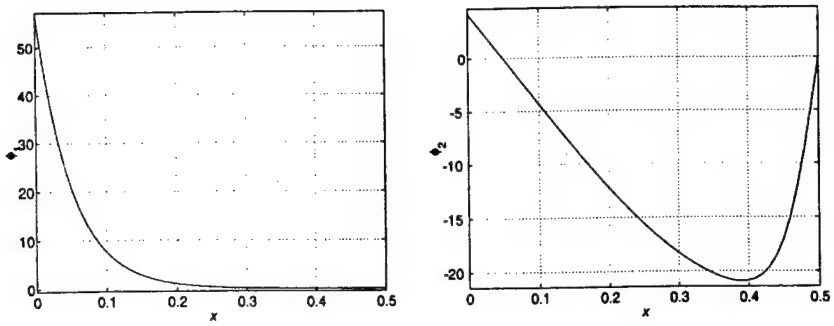

$\lambda_1 = .000323$ $\lambda_2 = -2732.95$

FIG. 20. Eigenfunctions with with $\gamma = 16$ (or $c_0 = 5.12$)

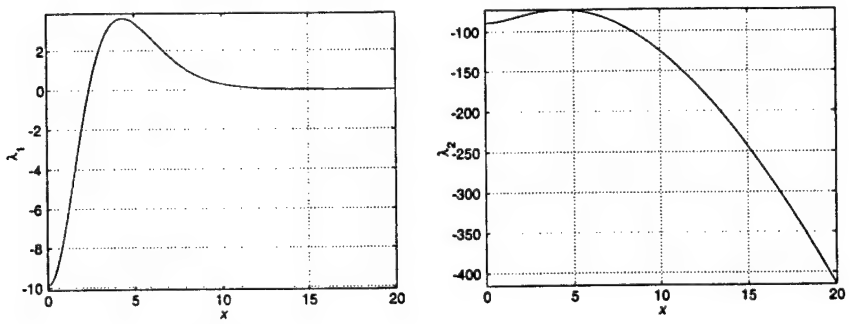

$\lambda_1 \times \gamma$ $\lambda_2 \times \gamma$

FIG. 21. Plot of Eigenvalues γ versus λ_j for $j = 1, 2$

The main thing we learn from this exercise is that the linearization is not exponentially stable for large values of c_0 and so the corresponding stationary solutions are not stable for the Burgers' system with nonhomogeneous Neumann boundary conditions. Nevertheless for a fixed floating point accuracy, as we have seen, the numerical solution to Burgers' equation, for certain anti-symmetric initial data, converge to the solution of this problem for some c_0.

5.2.10 Conclusions

In this paper we have shown that problem sensitivity and finite precision arithmetic can combine to produce false numerical solutions to steady state problems. Although one might guess that it is possible to construct pathological examples with this property, it is somewhat remarkable that this phenomenon can occur for a "simple" Burgers' equation. In addition, in the space of antisymmetric L^2 functions $L^2_{\mathrm{AS}}(0,1)$, we have shown that the steady state Burgers' equation has a unique solution ($v(x) = 0$), and yet, discretized versions of this equation can yield non-unique solutions. More importantly, for sufficiently large initial data, marching schemes will converge to this discrete (yet false) solution. We also presented a sensitivity and stability analysis that provides insight into these numerical difficulties.

One implication of these results is that more analysis needs to be done on recent "numerical based proofs" of nonuniqueness. In particular, we have established that in a perfectly reasonable model, numerical computations that yield nonunique discrete stationary

solutions do not imply anything about nonuniqueness for the continuous boundary value problem. It is important to again emphasize that it is finite precision arithmetic that causes these false solutions. Therefore, even converging an algorithm to machine roundoff error will not eliminate the difficulty.

Finally, we observe that the false numerical solutions can differ by orders of magnitude from real stationary solutions. Therefore, in such cases, cascading the numerical solutions into an optimization or control algorithm can produce bad designs. More about this issue will appear in future papers.

6 Report on the Cornell Subcontract

Partnership for Research Excellence and Transition (PRET) Contract
"Sensitivity and Adjoint Methods for Design of Aerospace Systems"
Virginia Polytechnic Institute and State University
Contract Number CR-19024-430662

FINAL REPORT
Cornell University
Contract Number 30049

Gahl Berkooz, Hal Carlson, John Lumley, Robert Miller

M&AE, Cornell University, Ithaca, NY 14853

6.1 Background and Objectives

The Partnership for Research Excellence and Transition (PRET) set as its goal to produce outstanding research and to work with industrial partners and Air Force partners to see that the research gets transitioned. Because of the nature of this project, the personnel working on it worked closely with the industrial partners. The strategy for assuring the success of the transition is that each postdoc was assigned as a "lead postdoc" for one industrial partner. It's the postdoc's job to assure that communication and research transition takes place.

Our proposal stated that we would use PDESolve as a generic tool for software development. BEAM was generous to provide PDESolve at no cost for use by PRET members.

The goal of the BEAM – Cornell transitions was to produce PDESolve modules for use by the PRET team and for applications to aerodynamic design and materials processing.

6.2 Research Achievements

This section contains a summary of the work preformed at Cornell.

6.2.1 High Level 3D Navier-Stokes Solver

We developed a 3D Navier Stokes solver using a Galerkin Least-Squares to circumvent the usual (LBB) div-stability restrictions on element pairs. A finite element mesh for this problem was created by post-processing a model generated in ProEngineer (a popular engineering 3D CAD package). A number of computational experiments for two dimensional flows were compared to published CFD solutions to verify the results of this software. , and implemented it in PDESolve.

Because of high level symbolic expression specifications of PDESolve the entire code was less than 200 lines long. This is very impressive because a similar code written using traditional techniques such as FORTRAN would have taken three years or more to write and would have consisted of tens of thousands of lines of code.

This effort pointed out a deficiency in certain aspects of PDESolve. Specifically, from this effort BEAM learned that the finite element engine underlying PDESolve needs to be significantly enhanced, perhaps even re-written if it is to support state-of-the-art DoD needs. This lesson was very valuable to BEAM.

This effort was also valuable in communicating to PRET members and potential DoD users and partners the power of mixed symbolic- numeric computing in general and PDE-Solve in particular.

As part of the Navier Stokes project, an evaluation of what geometric sensitivity information would need to be provided as boundary conditions for geometric sensitivity flow equations was done as well. This information was incorporated in the design of a 2D parametric geometry engine that provides sensitivity information as well as interfaces to 3D commercial geometry packages.

6.2.2 2D Shape Optimization and Optimization Architecture

BEAM Technologies developed a parametric 2D geometry engine that provides the information required for boundary conditions for geometry sensitivity partial differential equations. We applied this software to shape optimization model problems. The results were excellent; we were able to implement sensitivity and optimization very efficiently. We transitioned the lessons we learned to BEAM in the form of reccomendations for how to improve PDESolve in the areas of optimization.

Because computing cost function gradients is the key to any optimization algorithm, we developed an adaptive finite element strategy for computing cost function gradients efficiently and accurately. Using the continuous sensitivity equation, we were able to develop error estimates for sensitivity variables (derivatives of flow variables with respect to parameters) in addition to error estimates for the flow. Adaptive mesh refinement was performed to reduce both sets of errors. Thus, we were able to compute very accurate gradient calculations using fixed computing resources, or conversely, computationally efficient algorithms to obtain a desired level of gradient accuracy.

At the time of the research project, there were significant discussions in the community regarding the merits of the analytic sensitivities compared to automatic differentiation. Automatic differentiation has the advantage of being applicable to existing complex scientific and engineering codes, whereas analytic sensitivities offer improved speed (both targeted at computing cost function gradients.) To bridge this divide we developed a method for

Computation of continuous sensitivity equations by applying standard automatic differentiation software to (slightly) modified PDE solvers were demonstrated. Using this technique, we were able to use AD to compute derivatives of PDE solutions with respect to shape parameters without the need to compute derivatives of discretization parameters (such as the mesh, adaptive time stepping algorithm, etc.).

6.2.3 Sensor and Actuator Optimization in Flexible Structure Vibration Control

An area of importance to the Air Force and NASA at the time was the optimization of the location of sensors and actuators for smart structure control. In this application piezoelectric sensors and actuators are placed on a structure and a control algorithm is used to dampen the vibrations. This allows the reduction of the weight of a sattelite, for example. Using PDESolve we developed innovative technology to help address this question. This technology was transitioned to BEAM. Research included algorithms for modeling beams, plates, box beams, and three-dimensional elastic structures with distributed SMEC's (Smart Materials Embedded Components) for controlling vibration and stress. Piezoelectric actuators are modeled as three-dimensional, homogeneous bodies using the quasi-static linear theory of electroelasticity. Governing equations for the substrate structures and embedded components are expressed in finite-element formulations. The software employs model order reduction and has direct interfaces with control design software like Matlab and CAD software like ProEngineer. See attached report.

6.2.4 Materials Processing Applications of Relevance to the Air Force

Since one of the objectives of the Cornell - BEAM collaboration was to develop modules in the area of materials processing, an effort was put into identifying materials processing applications that may be of interest to BEAM on the one hand and are relevant to the Air Force on the other hand. Two applications were identified:

Injection molding of viscoelastic and viscoplastic materials As a result of collaboration with Allied Signal we learned that Allied Signal has developed a certain ceramic slurry that they were interested in injection-molding into shapes that would eventually become turbine blades after a baking process. Ceramic blades was an area DARPA made heavy investments in, and Allied Signal was one of the beneficiaries of these funds. However, despite the success in the development of the basic materials, Allied Signal had a problem with the manufacturing process. Specifically, optimization of the location of the material injection point was an issue. A collaborative effort was put in place to try and solve a generic 3D injection molding problem, followed by models with more complex material physics. This effort did not yield conclusive results, as PDESolve had difficulties in converging some of the problems.

Chemical Vapor Infiltration in the Manufacturing of Carbon-Carbon Composites

Carbon-Carbon composites is a technology the Air Force has made significant investments in. One of the problems with this technology is that setting manufacturing parameters is a trial and error process. The process is very expensive because each manufacturing run

may take up to a week of "baking." The objective of this work was to develop a capability to optimize the process. The first step was to set up a simulation of the process. This project was a great success – the symbolic nature of PDESolve enabled solving fully implicit chemistry using a species-sensitivity matrix. All the simulations were in 2D. This project again proved the power of a mixed symbolic-numeric approach. This was a collaborative effort with BEAM.

6.2.5 Fluid Structure Interaction

A new method for predicting dynamic effects of fluid-structure interaction was developed by BEAM, for the purpose of optimizing designs to minimize flutter, and enable the control of flutter with sensors and actuators. BEAM made several extensions to PDESolve, as well as a PDESolve code generator using *Mathematica*. These were provided to Cornell at no cost for the purpose of researching BEAM's new method and providing feedback to BEAM. The new method holds great promise, and is currently the only known approach that can account for viscous effects on flutter and limit cycle oscillations using CFD-quality fluid dynamics data. The results of this research are summarized in the papers by Miller.

6.2.6 Control and fluid Structure interaction

In work related to both flexible structure vibration control and to fluid structure interaction (see sections 6.2.3, 6.2.5) we examined the structure of the turbulent boundary layer with an eye to its control and modification over flexible structures. As a first step, we considered a compliant surface. Specifically, we followed an approach in which only the large scales of the boundary layer are resolved, the smaller scales being parameterized. In this way, a low-dimensional model of the layer is developed, which can be investigated dynamically as it interacts with various structures. The general approach is described in the papers below.

More general contributions are contained in the papers by Lumley and his co-workers. In particular, the book by Lumley describes the application of some of these same ideas to flow in engine cylinders. A tumbling flow leads to elliptic instability which promotes high turbulence, increasing flame speed and reducing pollution. Our approach permits the examination of this dynamical process and its manipulation to optimize these effects.

The second book by Lumley is a report on current interesting research directions in fluid dynamics prepared under the auspices of the U. S. National Committee on Theoretical and Applied Mechanics. This was intended for members of Congress and their staffs.

7 Honors

- Professor John Burns was named Hatcher Professor,
- Professor John Burns was elected Fellow of the IEEE,
- Professor Jeff Borggaard was named a PECASE Fellow,

8 Personnel Supported

The following people were supported in part under Grant F49620-96-1-0329:

Senior Investigators	Postdoctoral Fellows	Graduate Students
Gahl Berkooz	Hal Carlson	Jeanne Atwell
Jeff Borggaard	Robert Miller	Chris Camphouse
John Burns	Oliver Stein	Kevin Hulsing
Eugene Cliff	Paul Gilmore	Alejandro Limache
Matthias Heinkenschloss	Diana Rubio	Graciela Cerezo
Bernard Grossman	Chris Camphouse	Vinh Nguyen
Terry Herdman	Jeff Borggaard	Rajiv Sampath
Belinda King		Stefanie Feih
Yuying Li		Sandra Ham
John Lumley		Shana Olds
Dominique Pelletier		Ajit Shenoy
Ekkehard Sachs		Lisa Stanley
Nick Zabaras		Joseph Mugtussidis
		Mary Gallo
		Dawn Stewart
		Lyle Smith
		Ken Massa
		Eric Vugrin
		Denise Krueger
		Katie Camp

9 Interactions/Transitions

Our efforts to expedite the transition of our research to industrial and Air Force needs are manifested by direct industrial/laboratory interactions and participation at professional meetings. One of the major components of this effort was active cooperation and coordination with the Air Force Research Laboratory (AFRL) and with our industrial partners. We have actively worked with all of our industrial partners and with groups at AFRL/VACA and AFRL/DE.

Industry/Laboratory Interactions

Aerosoft Inc.
We worked closely with AeroSoft on several projects to develop software packages for analysis and design of aerospace systems. The central theme in these efforts is the continuous sensitivity equation method (SEM) for approximating the effect of parametric design changes on aerodynamic performance. As of this writing the production code *SENSE* is at Version 1.0.4. Recent additions permit sensitivity calculations in turbulent flows with one and two-equation turbulence models. We continue to support AeroSoft's work with AFRL/DE on design and analysis for COIL lasers. As noted above, we are studying formulations to efficiently couple single discipline sensitivity codes for the study of multi-physics problems. This work is being supported by AFRL/DE and is described below.

Boeing Defense and Space Group (BDSG)
Recent efforts with our Boeing partners are focused on transition of our recent work on CFD/Sensitivity methods for estimating rotary aerodynamic derivatives. Dr. A.C. Limache has completed his Ph.D. studies in this area and research is being transitioned to Boeing. Our initial objective is to implement required changes in a 3D Euler code to provide a capability to estimate aerodynamic forces and moments in a generalized steady flight maneuver.

Directed Energy Directorate of AFRL
Dr. T. J. Madden and others at (AFRL/DELC) are involved in efforts to develop technologies for improved performance in chemical oxygen-iodine lasers (COIL). Gaseous chemical lasers can provide lightweight, efficient energy sources for a wide variety of Air Force systems including airborne and space-based directed energy weapons. Computer-based design tools can lead to rapid development of efficient laser-power systems. In addition to the coupled sensitivity analyses noted above, we are developing an alternative formulation, based on a paraxial wave equation, for modeling energy extraction in the laser cavity. This replaces a "discrete" ray-tracing algorithm currently in use at AFRL/DELC and is a more natural setting for continuous sensitivity analysis.

Air Vehicles Directorate of AFRL
Dr. Siva Banda and others at AFRL/VACA are starting a new effort to develop control technologies for application to flow control. We are working with Dr. Banda's group on flow control and computational tools for design of distributed parameter systems. We plan to extend earlier work on functional gain computations to a practical experimental test. Dr. Burns will be spending time at AFRL/VACA to help initiate this project.

10 Publications Produced Under the Grant

Books

1. *Computational Methods for Optimal Design and Control*, Edited by Jeff Borggaard, John Burns, Eugene Cliff and Scott Schreck, Progress in Systems and Control Theory, Birkhäuser, Boston, 1998, 475 pages.

Journal Articles

1. Allen, E., Burns, J, Gilliam, D., Hill, J., and Shubov, V., *The Impact of Finite Precision Arithmetic and Sensitivity on the Numerical Solution of Partial Differential Equations*, Journal of Mathematical and Computer Modeling, 35 (2002), pages 1165-1196.

2. Atwell, J. A., and King, B. B., *Computational Aspects of Reduced Order Feedback Controllers using Proper Orthogonal Decomposition, Proc. 38th IEEE CDC, Phoenix AZ Dec. 7-10, 1999*, pages 4301 - 4306.

3. Atwell, J. A., and King, B. B., *Stabilized Finite Element Methods and Feedback Control for Burgers' Equation*, Virginia Tech ICAM Report 00-02-01; *Proc. of the 2000 American Control Conference*, pages 2745-2749.

4. Atwell, J.A. and King, B.B., *Proper Orthogonal Decomposition for Reduced Basis Controllers for Parabolic Systems*, Mathematical and Computer Modelling, 33 (2001), pages 1-19.

5. Aubry, N., Berkooz, G., Coller, B., Elezgaray, J., Holmes, P. J., Lumley, J. L. and Poje, A., Low dimensional models, wavelet transforms and control, in *Eddy structure identification*, ed. J.-P. Bonnet, Wien/New York: Springer, pp. 271–332, 1996.

6. Berkooz, G., Newsome , R. and Bjaskaran, R., *On Analytical Flow Sensitivities and their Use in the Calculation of Fluid-Structure Interaction*, AIAA Journal, Vol. 36. No. 8. (1998), 1537-1540.

7. Balogh, A., Burns, J., Gilliam, D. and Shubov, V., A Note on Numerical Stationary Solutions for the Viscous Burgers' Equation, *Journal of Math. Systems, Estimation, and Control*, Vol. 8, No. 2, 1998, 253–256. Full electronic manuscript published March, 1998, 16 pp. Retrieval code: 55578.

8. Berger, S., Burns, J., Burr, R. and Gilmore, P., Automated Optimization Techniques for Phase Change Piezoelectric Ink Jet Performance Enhancement, *1997 International Conference on Digital Printing Technologies*, Society for Imaging Science and Technology, IS&T's NIP13, November, 1997, 716–721.

9. Blossey, P. N. and Lumley, J. L., *Control of Intermittency in Near-Wall Turbulent Flow*, Intermittency in Turbulent Flows and Other Dynamical Systems, J. C. Vassilicos, Ed., The University Press, Cambridge, UK, in press.

10. Bhaskaran, R. and Berkooz, G., Optimization of Fluid-Structure Interaction Using the Sensitivity Equation Approach, *4th International Symposium on Fluid-Structure Interaction, Aeroelasticity, Flow-Induced Vibrations & Noise, ASME International Mechanical Engineering Congress & Exposition*, Nov 16-21 1997, Dallas, Texas, to appear.

11. Borggaard, J. and Burns, J., Asymptotically Consistent Gradients in Optimal Design, in *Multidisciplinary Design Optimization*, N. M. Alexandrov and M. Y. Hussaini, Ed., SIAM Publications, 303–314, 1997.

12. Borggaard, J. and Burns, J., A PDE Sensitivity Equation Method for Optimal Aerodynamic Design, *Journal of Computational Physics*, Vol. 136, pages 366–384, 1997.

13. Borggaard, J. and Pelletier, D., On Optimal Design Using an Adaptive Finite Element Method, in *Proceedings of the First International Conference on Nonlinear Problems in Aeronautics and Aerospace*, S. Sivasundaram editor, Embry-Riddle Aeronautical University Press, pages 33–40, 1997.

14. Borggaard, J. and Pelletier, D., *Shape Design Sensitivity Calculations with an Adaptive Finite Element Method*, AIAA Journal, in press.

15. Borggaard, J. and Pelletier, D., *On Adaptive Sensitivity Calculations for Optimal Shape Design*, Computational Methods in Applied Mechanics and Engineering, in press.

16. Borggaard, J. and Pelletier, D. and Turgeon, É., *A Study of Cooling Strategies in Thermal Processes*, Proceedings of the 38th AIAA Aerospace Sciences Meeting and Exhibit, Jan. 2000, AIAA Paper Number 2000-0563.

17. Borggaard, J. and Pelletier, D., *A Sensitivity Equation Method for Conduction and Phase Change Problems*, Nonsmooth/Nonconvex Mechanics (Nonsmooth Optimization and Applications Series, Volume 45), D. Gao, R. Ogden and G. Stavroulakis, Eds., Kluwer, pages 43-68, (2001).

18. Borggaard, J. and Verma, A., *On Efficient Solutions to the Continuous Sensitivity Equation Using Structured Automatic Differentiation*, SIAM Journal of Scientific Computing, vol. 22 (2001), pages 39-62.

19. J. Borggaard, D. Pelletier and É. Turgeon, *A Continuous Sensitivity Equation Approach to Optimal Design in Mixed Convection*, in Numerical Heat Transfer, Part A: Applications, Vol. 38, No. 8, pages 869-885 (2000)

20. Borggaard, J. and Pelletier, D., Observations in Adaptive Refinement Strategies for Optimal Design, in *Computational Methods for Optimal Design and Control*, J. Borggaard, J. Burns, E. Cliff and S. Schreck editors, Birkhäuser, pages 59–76, (1998).

21. J. Borggaard, D. Pelletier and É. Turgeon, *Parametric Uncertainty Analysis for Thermal Fluid Calculations*, in Journal of Nonlinear Analysis: Series A theory And Methods, (to appear)

22. J. Borggaard, W. Eppard, W. McGrory, A. Godfrey and E. Cliff, *Recent Advances in Numerical Techniques for the Design and Analysis of COIL Systems*, in Proceedings of the 31st AIAA Plasmadynamics

23. J. Borggaard, D. Pelletier and É. Turgeon, *A General Continuous Sensitivity Equation Formulation for Complex Flows*, in Proceedings of the 8th AIAA/USAF/NASA/ISSMO Symposium on Multidisciplinary Analysis and Design, AIAA Paper, number 2000-4732, September 2000.

24. J. Borggaard, D. Pelletier and É. Turgeon, *A Continuous Sensitivity Equation Method for Flows with Temperature Dependent Properties*, in Proceedings of the 8th AIAA/USAF/NASA/ISSM Symposium on Multidisciplinary Analysis and Design, AIAA Paper, number 2000-4821, (September 2000)

25. J. Borggaard, D. Pelletier and É. Turgeon, *Sensitivity and Uncertainty Analysis for Variable Property Flows*, in Proceedings of the 39th AIAA Aerospace Sciences Meeting and Exhibit, AIAA Paper, number 2001-0140 (2001)

26. J. Borggaard with D. Lacasse, D. Pelletier and É. Turgeon, *Adaptivity, Sensitivity and Uncertainty: Towards Standards in CFD*, in Proceedings of the 39th AIAA Aerospace Sciences Meeting and Exhibit, AIAA Paper, number 2001-0192 (2001)

27. J. Borggaard, D. Pelletier and É. Turgeon, *Application of a Sensitivity Equation Method to the k - ε Model of Turbulence*, in Proceedings of the 15th AIAA Computational Fluid Dynamics Conference, AIAA Paper, number 2001-2534, (2001)

28. J. Borggaard, D. Pelletier and É. Turgeon, *A General Continuous Sensitivity Equation Formulation for the k - ε Model of Turbulence*, in Proceedings of the 15th AIAA Computational Fluid Dynamics Conf., AIAA Paper, no. 2001-3000, (2001)

29. J. Borggaard, D. Pelletier and É. Turgeon, *A Continuous Sensitivity Equation Approach to Optimal Design in Mixed Convection*, in Proceedings of the 1999 AIAA Thermophysics Conference, AIAA Paper Number 99-3625 (1999).

30. J. Borggaard with S. Shah and M. L. Wolfe, *A Two-Dimensional Model for Simulating the Fate of Subsurface-Banded Nitrogen*, in Proceedings of the 1999 ASAE Annual International Meeting, ASAE Paper Number 99-2140 (1999).

31. Bradshaw, P., Launder, B. E. and Lumley, J. L. 1996. Collaborative testing of turbulence models. *J. Fluids Engineering*, 118:243–247.

32. Burns, J.A. and Hulsing, K., *Numerical Methods for Approximating Functional Gains in LQR Boundary Control Problems*, Journal of Mathematical and Computer Modeling, 33 (2001), 89-100.

33. Burns, J., Kang, S., Kachroo, P. and Ozbay, K., System Dynamics and Feedback Control Formulations for Real Time Dynamic Traffic Routing, *Journal of Mathematical and Computer Modeling*, Vol. 27, No. 9, 27–49, 1998.

34. Burns, J. and King, B.. A Note on the Mathematical Modelling of Damped Second Order Systems, *ournal of Math. Systems, Estimation, and Control*, Vol. 8, No. 2, 1998, 189–192. Full electronic manuscript published March, 1998, Retrieval code: 82674.

35. Burns, J.A., King, B.B. and Rubio, D., *On the Design of Feedback Controllers for a Convecting Fluid Flow via Reduced Order Modeling*, 1999 IEEE International Conference on Control Applications, December 1999, 1157-1162.

36. Burns, J.A., King, B.B. and Rubio, D., *Feedback Control of a Thermal Fluid Using State Estimation*, International Journal of Computational Fluid Dynamics, 11(1998), 93-112.

37. Burns, J.A., King, B. B. and Rubio, A.D., Regularity of Feedback Operators for Boundary Control of Thermal Processes, *First International Conference on Nonlinear Problems in Aeronautics and Aerospace*, S. Sivasundaram, Ed., Embry-Riddle Aeronautical Press, May, 1996, 67–73.

38. Burns, J.A. and Rubio, A.D., Control of the Boussinesq Equations in a Thermal Loop, *Applied Mechanics in the Americas*, Vol. VI, M. Rysz, L. Godoy and L. Suarez, Eds., University of Iowa Press, January 1997, 142–145.

39. Burns, J.A., King, B. B. and Stein, O., *Computational Methods for Identification and Control of Nanoscale Materials*, in Proc. Mathematical Theory of Networks and Systems (MTNS) 2000, June 2000, paper S121-A7.

40. Burns, J. A., Morin, P., and Spies, R., *Parameter Differentiability of the Solution of a Nonlinear Abstract Cauchy Problem*, JMAA, 252 (2000), 18-31.

41. Burns, J.A. and Stanley, L., *A Note on the Use of Transformations in Sensitivity Computations for Elliptic Systems*, Journal of Mathematical and Computer Modeling, 33 (2001), 101-114.

42. Burns, J., Stanley, L. and Stewart, D., A Projection Method for Accurate Computation of Design Sensitivities, *Optimal Control: Theory, Algorithms, and Applications*, W.W. Hager and P.M. Pardalos, Eds., Kluwer Academic Press, 1998, 40–66.

43. Carlson, H. & Miller, R. 2001. An Eigensystem for Predicting and Controlling Unsteady Aeroelastacity. AIAA Paper 2001-0854, AIAA, Aerospace Sciences Meeting and Exhibit, 39th, Reno, NV, Jan. 8-11, 2001.

44. Carlson, H. A. and Lumley, J. L., Flow over an obstacle emerging from the wall of a channel. *AIAA J.*, 34(5):924–931, 1996.

45. Carlson, H. A. and Lumley, J. L Active control in the turbulent boundary layer of a minimal flow unit, *J. Fluid Mechanics*, in press.

46. Chen, H., Hatch, A., Peters, G., Pritchett, L., Stanley, L. and Scheprov, A. Pressure Tube Modeling Problem, in *1997 Industrial Mathematics Modeling Workshop for Graduate Students*, F. Reitich, J. Scroggs, and H. Tran, Eds., Raleigh, NC, 1998, 11–25.

47. Chiang, S., Herdman, T. and Turi, J., Numerical Methods for Singular Intregrodifferential Equations of Neutral Type, Proc. 15th IMACS World Congress on Scientific Computation, Modeling and Applied Mathematics, Vol. 2, A. Sydow ed., Wissenschaft and Technik, Verlag, Berlin, pp. 465–468, 1997.

48. Cliff, E.M., Heinkenschloss, M. and Shenoy, A., Adjoint-Based Methods in Aerodynamic Design-Optimization, in *Computational Methods in Optimal Design and Control*, J. Borggaard, J. Burns, E. Cliff, and S. Schreck, eds, Birkhauser-Boston, 1998, 91–112.

49. Cliff, E. M., Heinkenschloss, M. and Shenoy, A., An Optimal Control Problem for Flows with Discontinuities, *Journal of Optimization Theory and Applications*, Vol. 94, pp. 273–309, 1997.

50. Cliff, E. M., Heinkenschloss, M. and Shenoy, A., On the Optimality System for a 1D Euler Flow Problem, *Proceedings of the AIAA 6th Symposium on Multidisciplinary Analysis and Optimization*, AIAA Paper 96–3993, September 1996.

51. E. M. Cliff and A. Limache, *Aerodynamic Sensitivity Theory for Rotary Stability Derivatives*, J. of Aircraft, Vol. 37, No. 4, July 2000, pp. 676-683.

52. E. M. Cliff, J. B. Borggaard and W. M. Eppard, *Sensitivity Tools for Chemical Laser Systems*, IEEE Conference on Control Applications, Anchorage, AK, Sept. 2000, 8 pp

53. E. M. Cliff and A. G. Godfrey, *Sensitivity Equations for Turbulent flows*, AIAA paper 2001-1060, Aerospace Sciences Meeting, Reno NV, Jan 2001, 15 pp

54. Dadone, A. and Grossman, B., *Progressive Optimization of Inverse Fluid Dynamic Design Problems*, Computer and Fluids, in press.

55. Dadone, A. and Grossman, B., *Rapid Convergence of 2D Fluid Dynamic Design Problems Using Progressive Optimization*, Proceedings of the Sixteenth International Conference on Numerical Methods in Fluid Dynamics, Arcachnon, France, July 1998, Lecture Notes in Physics, 515, Ed: C.-H. Bruneau, Springer, 25–30.

56. Dadone, A. and Grossman, B., *CFD Design Problems Using Progressive Optimization*, Proceedings of the AIAA 14th Computational Fluid Dynamics Conference, Paper No. 99-3295-CP, Norfolk, VA, June 1999.

57. Dadone, A., Valorani, M. and Grossman, B., Optimization Methods of 2D Fluid Design Problems with Non-smooth or Noisy Objective Functions, Proceedings of ECCOMAS 96, Paris, France, September 9-13, 1996, in *Computational Fluid Dynamics '96*, John Wiley & Sons, Ltd., pp. 425–430.

58. Gablonsky, J., Hulsing, K., McShine, L., Pihlaja, A., Seshaiyer, P. and Settumba, N., Sipe Consolidation in Tire Design, in *1997 Industrial Mathematics Modeling Workshop for Graduate Students*, F. Reitich, J. Scroggs, and H. Tran, Eds., Raleigh, NC, February 1998, 26–35.

59. Gatski, T. B., Hussaini, M. Y. and Lumley, T. B. (eds.) *Simulation and Modeling of Turbulent Flows* New York/Oxford: Oxford U. P., 1996.

60. Giunta, A. A., Balabanov, V., Grossman, B., Mason, W. H., Watson, L. T. and Haftka, R. T., Multidisciplinary Design Optimization of a High-Speed Civil Transport, in *Proceedings of the Society of Engineering Science 33rd Annual Technical Meeting*, Arizona State University, Tempe, AZ, Oct. 1996.

61. Godfrey, A.G. and Cliff, E.M., Direct Calculation of Aerodynamic Force Derivatives: A Sensitivity Equation Approach, AIAA-98-0393, *AIAA Aerospace Sciences Meeting*, Reno, NV, 12–15 January 1998.

62. Godfrey, A.G., Eppard, W.M. and Cliff, E.M., *Using Sensitivity Equations for Chemically Reacting Flows*, AIAA-98-4805, 7th AIAA/USAF/ NASA/ ISSMO Symposium on Multidisciplinary Analysis and Optimization, St. Louis, MO, 2 - 4 September 1998, 10 pages.

63. Hartung, F., Herdman, T. and Turi, J., On the Existence, Uniqueness and Numerical Approximations for Neutral Equations with State Dependent Delays, *Journal of Applied Numerical Mathematics*, 24:393–409, 1997.

64. Hartung, F., Herdman, T. and Turi, J., Parameter Identification in Classes of Hereditary Systems of Neutral Type, *Journal of Applied Mathematics and Computation*, 89:147–160, 1998.

65. Hartung, F., Herdman, T. and Turi, J., *On Differentiability of Solutions with respect to Parameters in State-Dependent Delay Equations*, Journal of Nonlinear Analysis, 39 (3), 2000, 305-325.

66. Heinkenschloss, M. Projected Sequential Quadratic Programming Methods, *SIAM J. on Optimization*, Vol. 6, 1996, pp. 373–417.

67. Herdman, T. and Kang, K., Structured Reduced Sequential Quadratic Programming and its Application to a Flow Matching Problem, *First International Conference on Nonlinear Problems in Aeronautics and Aerospace*, S. Sivasundaram, Ed., Embry-Riddle Aeronautical Press, May, 1996, 255–262.

68. Herdman, T., Morin, P. and Spies, R., *Convergent Spectral Approximations for the Thermomechanical Processes in Shape Memory Alloys*, Journal of Nonlinear Analysis, 39 (1), 2000, 11-32.

69. Herdman, T., Morin, P. and Spies, R., *Parameter Identification for Nonlinear Abstract Cauchy Problems using Quasilinearization*, Journal of Optimization Theory and Applications, to appear.

70. Herdman, T., Morin, P. and Spies, R., *A Terminal Control Problem on the Dynamics of Shape Memory Alloys*, Nonlinear Problems in Aviation and Aerospace, to appear.

71. Herdman, T. L., Cereo,G., Fernandez, E. and Turi, J., *Numerical Identification Techniques for Singular Neutral Functional Differential Equations*, Nonlinear Problems in Aviation and Aerospace, Editor, S. Sivasundaram, Vol. 1, pages. 163-167. (2001)

72. Herdman, T., Morin, P. and Spies, R., *Modal Approximations for the Dynamics of Shape Memory Alloys under External Thermomechanical Actions*, Proc. 3rd International Conference on Nonlinear Problems in Aviation and Aerospace, Editor, S. Sivasundaram, Vol. 1, pp. 303-316 (2001).

73. Holmes, P. J., Lumley, J. L and Berkooz, G., Turbulence, Coherent Structures, Symmetry and Dynamical Systems. Cambridge, UK: University Press, in Press.

74. Holmes, P. J., Lumley, J. L., Berkooz, G., Mattingly, J. C. and Wittenberg, R. W., Low-dimensional models of coherent structures in turbulence, *Physics Reports*, submitted.

75. Ignat, L., Pelletier, D., and Ilinca, F., *Solution of Two-equation Models of Turbulence using a Universal Adaptive Finite Element Algorithm*, Proceedings of the 36th Aerospace Sciences Meeting & Exhibit, Jan. 1998, Reno, NV AIAA-98-0765.

76. King, B. B., *Representation of Feedback Operators for Parabolic Control Problems, Proceedings of the American Mathematical Society*, 128(2000), 1339-1346.

77. King, B.B., *Nonuniform Grids for Reduced Basis Design of Low Order Feedback Controllers for Nonlinear Continuous Systems*, Mathematical Models and Methods in Applied Sciences, Vol. 8, 1998, 1223–1241.

78. King, B.B., *Sensor Design for Compensator Based Control of a PDE System*, Proceedings of the 4th International Conference on Optimization Techniques and Applications, Perth, Australia, July 1–3, 1998, 352–359.

79. King, B.B. and Sachs, E.W., *Semidefinite Programming Techniques for Reduced Order Systems with Guaranteed Stability Margins*, Computational Optimization and Applications, in press.

80. King, B.B. and Sachs, E.W., Optimization Methods for Stable Reduced Order Partial Differential Equations, *Optimal Control: Theory, Algorithms, and Applications*, W.W. Hager and P.M Pardalos, eds., Kluwer Academic Publishers B.V, in press.

81. King, B.B. and Sachs, E.W., Reduced Order Controllers for Partial Differential Equation Systems with Guaranteed Stability Margins, *Proceedings of the 36th IEEE Conference on Decision and Control*, San Diego, CA, IEEE, December 1997, pp. 2219–2224.

82. Kleis, D., and Sachs E.W., *Optimal Control of the Sterilization of Prepackaged Food*, SIAM J. Optimization, in press.

83. Knill, D. L., Balabanov, V., Golividov, O., Grossman, B., Mason, W. H., Haftka, R. T. and Watson, L. T., Accuracy of Aerodynamic Predictions and Its Effects on Supersonic Transport Design, MAD Center Report 96-12-01, Virginia Tech, AOE Dept., Blacksburg, VA, Dec. 1996.

84. Limache, A. and Cliff, E.M., *Aerodynamic Sensitivity Theory for Rotary Stability Derivatives*, AIAA-99-4313, Atmospheric Flight Mechanics Conference, Portland, OR, 9 - 11 August 1999.

85. Lumley, J. L., *Some comments on the last hundred years of density fluctuations*, in Proceedings of the International Conference on Variable Density Turbulent Flows, eds. F. Anselmet, P. Chassaing L. Pietri. pp.1 -12. Perpignan: Presses Universitaires, 2000.

86. Lumley, J. L., *Early work on Fluid Mechanics*, in IC Engine. Annual Review of Fluid Mechanics, 33 (2001). pages 319-338.

87. Lumley, J. L., Acrivos, A., Leal, G. and Leibovich, S. (eds), *Research Trends in Fluid Dynamics*, Woodbury, NJ: AIP Press, 1996.

88. Lumley, J. L., Berkooz, G., Elezgaray, J., Holmes, P. J., Poje, A. and Volte, C., *Fundamental aspects of incompressible and compressible turbulent flows*, in Simulation and Modeling of Turbulent Flows, eds. T.B. Gatski, M. Y. Hussaini and J. L. Lumley. New York/Oxford: Oxford U. P. pp. 5–78, 1996.

89. Lumley, J. L. and Poje, A., *Low-dimensional models for flows with density fluctuations*, The Physics of Fluids, 9(7): 2023–2031, 1997.

90. Lumley, J. L, *Prediction Methods in Turbulence*, Future Strategies Toward Understanding and Prediction of Turbulent Systems, G. F. Hewitt and M. W. Reeks, Eds., The University Press, Cambridge, UK, in production.

91. Lumley, J. L., Blossey, P. N. and Podvin-Delarue, B., *Low dimensional models, the minimal flow unit and control*, In Fundamental Problematic Issues in Turbulence, ed. A. Gyr, W. Kinzelbach and A. Tsinober. 57-66. Trends in Mathematics. Basel: Birkhauser, 1999.

92. Lumley, J. L., Blossey, P. N., *The low dimensional approach to turbulence.* In Modeling Complex Turbulent Flows, eds. M.D. Salas, J. Hefner and L. Sakell. 89-106. Dordrecht: Kluwer, 1999.

93. Lumley, J. L., *Engines: An Introduction.* New York: Cambridge University Press, 1999.

94. Lumley, J. L., Blossey, P. N., *Reduced-order modeling and control of near-wall turbulence*, Proceedings 38th IEEE Conference on Decision and Control, Phoenix, Arizona, December 7-10, 1999.

95. Lumley, J. L., Yang, Z., and Shih, T. H., *A Length Scale Equation*, Dordrecht:Kluwer. 60th Birthday of Brian Launder, in Flow, Turbulence and Combustion. 63:1-21.

96. Lumley, J. L., (Ed.), *Fluid Mechanics and the Environment: Dynamical Approaches*, Heidelberg: Springer Verlag. In press.

97. Lumley, J. L. and Yaglom, A, *A century of turbulence*, in Advances in Turbulence VIII, ed. C. Dopazo. (2000), pp. 3-12, Barcelona: CIMNE.

98. McGrory, W., Eppard, M. and Godfrey, A., *Recent Advances in Numerical Techniques for the Design and Analysis of COIL Lasers*, AIAA Paper 2000-2576, AIAA Plasmadynamics and Lasers Conference, June 2000.

99. Mugtussidis, I. and Cliff, E. M., A New Dynamic Model to Assess Aircraft Agility, in *Proceedings of AIAA Atmospheric Flight Mechanics Conference*, August, 1997, New Orleans, LA, pp. 328–338. (AIAA Paper Number 97-3584).

100. Parsons, L. M., Rempfer, D. & Lumley, J. L., *Low-dimensional modeling of near-wall turbulence - compliant boundary interaction*, Physics of Fluids. Submitted.

101. Pelletier, D., *Should We Still Teach CFD to Our Students*, Proceedings of the 36th Aerospace Sciences Meeting & Exhibit, Jan. 1998, Reno, NV AIAA-98-0824.

102. Pelletier, D., Borggaard, J. and Hétu, J.-F., *A Continuous Sensitivity Equation Method for Conduction and Phase Change Problems*, in Proceedings of the 38th AIAA Aerospace Sciences Meeting and Exhibit, Jan. 2000, AIAA Paper Number 2000-0881.

103. Phillips, W. R. C., Wu, Z. and Lumley, J. L., On the formation of longitudinal vortices in a turbulent boundary layer over wavy terrain. *J. Fluid Mech.* 326: 321–341, 1996.

104. Podvin, B., Lumley, J. L. and Berkooz, G., Non-linear Kalman filtering for a turbulent channel flow. *AIAA Journal*, in review.

105. Podvin, B. and Lumley, J. L., A low-dimensional approach to the minimal flow unit, *J. Fluid Mech*, in review.

106. Podvin, B., Gibson, J., Berkooz, G. and Lumley, J. L., Lagrangian and Eulerian view of the bursting period, *The Physics of Fluids*, in press.

107. Podvin, B. and Lumley, J.L., Reconstructing the flow in the wall region from wall sensors, *The Physics of Fluids*, in review.

108. Rubio, D., Boundary Control for the Chaotic Flow of a Thermal Convection Loop, *Proceedings of the 34th IEEE Conference on Decision and Control*, New Orleans, December, 1996, pp. 3734–3737.

109. Shenoy, A., Heinkenschloss, M. and Cliff, E.M., *Airfoil Design by an All-at-Once Method*, International Journal of Computational Fluid Dynamics, Vol. 11, 1998, pages 3 - 25.

110. Shih, T.-H., Zhu, J. and Lumley, J.L., Calculation of Wall-Bounded Complex Flows and Free Shear Flows, *International Journal for Numerical Methods in Fluids*, 23:1133-1144, 1996.

111. Shih, T.-H., Zhu, J., Liou, W., Chen, K.-H., Liu, N.-S. and Lumley, J. L., Modeling of turbulent swirling flows, NASA Contractor Report, Lewis Research Center, 1997.

112. Stanley, L.G. and Stewart, D.L. A Comparison of Local and Global Projections in Design Sensitivity Computations, in *Computational Methods for Optimal Design and Control*, J. Borggaard, J. Burns, E. Cliff, and S. Schreck, Eds., Birkhauser-Boston, 1998, 59–76.

113. Xu, S., Rempfer, D. and Lumley, J. L.,*Numerical simulation of turbulent skin friction reduction by wall compliance*. J. Fluid Mech. Submitted.

114. Yang, G. and Zabaras, N., *The Adjoint Method for an Inverse Design Problem in the Directional Solidification of Binary Alloys*, Journal of Computational Physics, Vol. 140, 1998, 432-452.